BLADE SCALE EFFECTS OF TIP LEAKAGE

by

M. Martinez-Sanchez and R.P. Gauthier

GTL Report #202 October 1990

GAS TURBINE LABORATORY
MASSACHUSETTS INSTITUTE OF TECHNOLOGY
CAMBRIDGE, MASSACHUSETTS

BLADE SCALE EFFECTS OF TIP LEAKAGE

by

M. Martinez-Sanchez and R.P. Gauthier

GTL Report #202 October 1990

This research was supported by NASA Marshall SFC under Contract No. NAS8-35019
(Glenn E. Wilmer, Technical Monitor).

BLADE-SCALE EFFECTS OF TIP LEAKAGE

by

M. Martinez-Sanchez and R.P. Gauthier

MIT Gas Turbine Laboratory

ABSTRACT

The effects of blade-tip leakage in a turbine are investigated by modeling the stage as an incomplete actuator disk. It is found that the spanwise flow redistribution due to the gap is such as to produce a uniform unloading of the blades, despite the very concentrated leakage. Partial lift retention at the blade tip is accounted for based on a leakage jet-free stream collision model which successfully predicts the roll-up of the leakage flow. The predicted efficiency loss due to the gap correlates well with experimental data.

1. Introduction

The effects of the finite gap at the tip of the blades of various kinds of turbomachinery has long been a topic of study, both theoretical and experimental, motivated largely by its strong impact on stage performance. An additional motivation arises, in our case, from the role of blade-tip losses in the generation of de-stabilizing cross forces on turbine disks. The mechanism for these forces, as first proposed by Alford[1] and Thomas[2], is depicted in Fig. 1. It is an empirical observation that the efficiency of a turbine decreases more or less linearly with the ratio of tip gap to blade height:

$$\eta = \eta_o - \beta \frac{\delta}{H} \tag{1}$$

where β is a numerical factor of order 1-2. Re-writing in terms of the force f per unit azimuthal length,

$$\frac{f}{f_{IDEAL}} = \frac{f_o}{f_{IDEAL}} - \beta \frac{\delta}{H} \tag{2}$$

If a turbine disk with mean gap $\bar{\delta}$ is offset by e_x in the transverse Ox direction, then, measuring azimuth θ from the point where the gap is maximum,

$$\delta(\theta) = \bar{\delta} - e_x \cos\theta \tag{3}$$

We can now project all forces in the OY direction, (perpendicular to the offset), to obtain $f_y = f \cos\theta$ per unit length, for a total cross-force $F_y = \int_o^{2\pi} f_y R \, d\theta$. Using Eqs. (2) and (3),

$$F_y = \beta \frac{e_x}{H} f_{IDEAL} \pi R$$

or, noting that the ideal torque is $Q_{IDEAL} = 2\pi R^2 f_{IDEAL}$,

$$F_y = \frac{\beta}{2}\left(\frac{Q_{IDEAL}}{R}\right)\left(\frac{e_x}{H}\right) \qquad (4)$$

This force is only opposed by inertia and damping forces, since the structural restoring reactions to e_x would normally act along Ox. The result, if damping is insufficient, is a divergent whirling motion. Equation (4) shows the importance of the loss factor β (Eq. (1)) for prediciton of the stability properties of a rotor.

The extensive data base on tip-loss factors has been correlated by many authors on the basis of various levels of analysis. A good review of these efforts was presented by Waterman[3], from whose paper we have borrowed Fig. 2. Waterman selected 10 well documented turbine test cases and five tip-loss prediction schemes, and obtained results which are statistically summarized in Table 1, also taken from Ref. 3. (Results based on Lakshminarayana's method were omitted because of their systematic overpredictions). Given that β averages roughly 1.5, the variances in the first column of Table 1 indicate a fairly unsatisfactory state of affairs regarding predictive capabilities. Perhaps at the root of this situation is the lack of a clear model of how the losses arise. Generally speaking, the various approaches used have fallen into three categories:

(a) Models based on calculation of the pressure-driven tip gap flow rate, plus the assumption that some portion of the kinetic energy of this flow is lost. Various corrections are used for viscous and other effects. The models of Rains[4] and Vavra[5] are in this category.

(b) Models based on adaptations of wing theory to predict the "induced drag" produced by the trailing vorticity escaping at each blade tip. A key difficulty is the predicition of tip lift retention, which determines the strength of such vortices. Examples are Lakshminarayana[6],[7] and Lewis and Yeung[8].

(c) More recently, detailed 2 and 3 dimensional numerical computaions of flow in a passage, including gap effects, have become possible[9],[10]. While these give important insight as to many details of the flow pattern, they still lack the precision required to calculate the

small deficits which add up to the losses. This is not unlike the situation regarding a much better explored problem, i.e., drag predicitions on a 2-D airfoil.

The models in Group (a) above are basically correct as to gap flow predictions, and can be regarded as a satisfactory first order description of near-gap effects. On the other hand, they ignore the concomitant small changes to the flow over the rest of the blade when a small gap is present. We will show later that it is these changes that are responsible for most of the blade force losses.

The models of Group (b), with their emphasis on induced drag, come closer to capturing the essence of the phenomenon. Indeed, the flow disturbances at the blades induced by trailing vortices can be one way of describing the blade-scale effects of tip leakage. What has been lacking is a globally consistent model of the strength and distribution of these vortices. Thus, Lakshminarayana[6] used an array of straight-line trailing vortices of uniform strength, equal to an empirically determined fraction of the blade lift. Ad-hoc corrections for vortex roll- up[7] improve the details of blade pressure distributions with little positive impact on loss prediction.

In this work, we emphasize the global nature of the blade-tip problem by using an actuator disk model for the stage. Details of the near-blade flow are in this way simplified by being relegated to the role of algebraic connecting conditions between the upstream and downstream flows. On the other hand, the spanwise rearrangement of the flow pattern due to preferential migration towards the gap region can be correctly captured, provided one recognizes the discontinuous nature of the downstream velocity distribution (i.e., the presence of a shear layer along the tip streamsurface). This shear layer is, of course, he result of azimuthally smearing the individual "trailing vertices" of the blades. With some reasonable mathematical approximations, results can be obtained from this model which agree with data to an equal or greater extent than existing correlations. Perhaps more

importantly, these results are easily enough related to the basic nature of the problem that generalization appears possible to include effects such as non-uniform gap distributions (our principal goal) or non-uniform inlet flow. Improvements can also be introduced on the details of the flow on the gap scale to account for partial tip loading, as will be discussed.

2. FORMULATION

For maximum simplicity, our initial model will make the following assumptions, some of which will be later relaxed:

(a) Imcompressible, inviscid flow

(b) Two-dimensional geometry

(c) Uniformity along the tangential (y) direction

(d) Fluid passing through the rotor blade-tip gap does no work.

(e) Stage collapsed in the axial directon to a single plane, and smeared in the azimuthal direction.

The "actuator disk" which represents the stage consists of a full-span stator and a partial-span rotor (Fig. 3), both occupying the x = o plane. Since there are no variations with y, the azimuthal momentum equation reads

$$c_x \frac{\partial c_y}{\partial x} + c_z \frac{\partial c_y}{\partial z} = o \tag{5a}$$

or, introducing the vector $\vec{c}_\perp = \vec{i}c_x + \vec{k}c_z$ to represent the meridional velocity projection,

$$\vec{c}_\perp . \nabla c_y = o \tag{5b}$$

showing that $c_\perp$ is simply convected by $\vec{c}_y$. Similarly, the vorticity equation reduces in this case to

$$\vec{c}_\perp . \nabla \omega_y = o \tag{6}$$

where

$$\omega_y = \frac{\partial c_x}{\partial z} - \frac{\partial c_z}{\partial x} \tag{7}$$

and the Bernoulli equation reduces to

$$\vec{c}_\perp . \nabla B_\perp = o \tag{8}$$

where

$$B_\perp = \frac{P}{\rho} + \frac{1}{2} c_\perp^2 \tag{9}$$

Continuity is satisfied by introducing the stream function $\Psi(x,z)$ for the meridional flow:

$$c_x = \frac{\partial \Psi}{\partial z} \quad ; \quad c_z = -\frac{\partial \Psi}{\partial x} \tag{10a,b}$$

and then Eqs. (5b), (6) and (8) reduce to

$$c_y = c_y(\Psi) \tag{11}$$

$$\omega_y = \omega_y(\Psi) \tag{12}$$

$$B_\perp = B_\perp(\Psi) \tag{13}$$

Using in Eq. (12), the definitions in Eqs. (7) and (10) produce the equation which governs $\Psi(x,z)$:

$$\nabla^2 \Psi = \omega_y(\Psi) \tag{14}$$

where, in this case, $\nabla^2 = \nabla_\perp^2 = \frac{\partial^2}{\partial x^2} + \frac{\partial^2}{\partial z^2}$.

Notice that the meridional flow (c_x, c_z) is decoupled from c_y, and can be solved for first. The component c_y, as well as $\omega_x = -\frac{\partial c_y}{\partial z}$, $\omega_z = \frac{\partial c_y}{\partial x}$, can be found a-posteriori.

Upstream of the stage ($x < o$), we assume the flow is irrotational ($\omega_y = o$), and Ψ simply obeys Laplace's equation. Uneven work extraction as the flow goes through the stage gives rise to non-zero vorticity ω_y downstream of the disk, and the value of ω_y is carried unchanged on each streamline from here on.

The vorticity ω_y and the meridional Bernoulli constant, $B_\perp$ are related to each other in a simple way. Starting from the Lamb form of the meridional momentum equation,

$$\nabla B_\perp + \omega_y \vec{k} \times \vec{c}_\perp = 0 \qquad \left(\vec{k} = \frac{\vec{\omega_y}}{\omega_y}\right)$$

and taking the cross-product with $\vec{c}_\perp$,

$$\omega_y = -\frac{1}{c_\perp^2}\vec{c}_\perp \times \nabla B_\perp \tag{15}$$

Remembering that, $B_\perp = B_\perp(\Psi)$we have $\nabla B_\perp = \left(\frac{dB}{d\Psi}\right)\nabla\Psi$, and $(\vec{c}_\perp \times \nabla B_\perp)_y = \left(\frac{dB}{d\Psi}\right)(\vec{c}_\perp \times \nabla\Psi)_y$. From the definition of Ψ (Eq. 10),

$(\vec{c}_\perp \times \nabla\Psi)_y = -c_\perp^2$, so that

$$\omega_y = \frac{\partial B_\perp}{\partial \Psi} \tag{16}$$

This relationship opens the way for a connection between the downstream ω_y and the non-uniformity of extracted work at the disk. Let subscripts 1 and 3 denote stations just upstream and just downstream of the stage (Fig. 3). Them because of continuity,

$$c_{x_3} = c_{x_1} \tag{17}$$

and, since we assume spanwise uniform blading, which can exert no forces on the flow in the z-direction,

$$c_{z_3} = c_{z_1} \tag{18}$$

Because of (17), (18) and the definition (9),

$$B_{\perp_1} - B_{\perp_3} = \frac{P_1 - P_3}{\rho} \tag{19}$$

Now, upstream of the stage, the absence of vorticity implies $\frac{dB_{\perp_1}}{d\Psi} = 0$ and so, from (16),

$$\omega_y = \frac{dB_{\perp_3}}{d\Psi} = -\frac{d(B_{\perp_1} - B_{\perp_3})}{d\Psi} = -\frac{d}{d\Psi}\left(\frac{P_1 - P_3}{\rho}\right) \tag{20}$$

which gives the vorticity ω_y when the distribution of (isentropic) static enthalpy extraction $\left(\frac{P_1 - P_3}{\rho}\right)$ is known.

The geometry of the stage blading is shown in Fig. 4. Euler's equation gives for the stagnation enthalpy decrease across the stage

$$-\Delta h_t = U\left[c_x \tan \alpha_2 - (U - c_x \tan \beta_3)\right] \tag{21}$$

where U is the wheel speed.

Adding to this the kinetic energy increase

$$\Delta \text{ (K.E.)} = \frac{1}{2} c_{y_3}^2 = \frac{1}{2} (U - c_x \tan \beta_3)^2 \tag{22}$$

we obtain, for any streamline which crosses the disk in the region covered by the blades (not the gap)

$$\left(\frac{P_1 - P_3}{\rho}\right)_{BL} = U c_x \tan \alpha_2 - \frac{1}{2}(U^2 - c_x^2 \tan^2 \beta_3) \tag{23}$$

Exactly how much work is extracted from those streamlines which at some point cross the blade-tip gap is a relatively complicated question to answer, and to which we will return in Sections 8,9. For now, we will make the simplest possible approximation, namely, that no work is extracted. This implies for such streamlines

$$\left(\frac{P_1 - P_3}{\rho}\right)_{GAP} = \frac{P_1 - P_2}{\rho} = \frac{1}{2} c_x^2 \tan^2 \alpha_2 \tag{24}$$

In Eqs. (23), (24), the axial velocity c_x at the disk is to be regarded as a function of z, in anticipation of redistribution of the flow in response to the presence of the gap. When using Eqs. (20), therefore, we will put

$$\frac{d}{dx} = \frac{\partial}{\partial c_x}\left(\frac{\partial c_x}{\partial z}\frac{\partial z}{\partial \Psi}\right)_{x=0} = \left(\frac{1}{c_x}\frac{\partial c_x}{\partial z}\right)_{x=0}\frac{\partial}{\partial c_x}$$

and so the ω_y vorticity can be calculated from Eqs. (23,) (24) as

BLADES: $$\omega_y = -\left[\frac{U}{(c_x)_{x=0}} \tan \alpha_2 + \tan^2 \beta_3\right]\left(\frac{\partial c_x}{\partial z}\right)_{x=0} \qquad (25a)$$

GAP: $$\omega_y = -\tan^2 \alpha_2 \left(\frac{\partial c_x}{\partial z}\right)_{x=0} \qquad (25b)$$

Since there is a discontinuity in the connecting conditions for flow through the gap versus flow through the blade passages, we can also expect a discontinuity, in the form of a shear layer, on the downstream portion of the streamline which passes through the blade ips. Denoting by superscripts (+) and (-) the regions on the gap and blade side of this layer, respectively, (Fig. 4a) its strength (at least for the y -component) will be

$$Q = \int_{-}^{+} \omega_y \, d\Psi = B_{\perp_3}^{+} - B_{\perp_3}^{-} \qquad (26)$$

With the help of Eqs. (19), (23) and (24), and the fact that no discontinuity exists in $B_{\perp_1}$ we obtain

$$Q = U c_x^{-} \tan \alpha_2 - \frac{1}{2}\left(U^2 - c_x^{-2} \tan^2 \beta_3\right) - \frac{1}{2} c_x^{+2} \tan^2 \alpha_2 \qquad (27)$$

Recapitulating, the equation for Ψ is

UPSTREAM: $$\nabla^2 \Psi = 0 \qquad (28a)$$

DOWNSTREAM $\left\{ \begin{matrix} \text{GAP} \\ \text{BLADES} \end{matrix} \right\}$:

$$\nabla^2\psi = \left\{ \begin{matrix} -\tan^2 \alpha_2 \\ -\left[\frac{U}{(c_x)_{x=0}} \tan \alpha_2 + \tan^2 \beta_3\right] \end{matrix} \right\} \left(\frac{\partial c_x}{\partial z}\right)_{x=o} + Q\,\delta(\Psi - \Psi_{TIP})$$

Where $\delta(\Psi - \Psi_{TIP})$ is Dirac's delta function

The boundary conditions are

$$\Psi(x,o) = o \quad ; \quad \Psi(x, H) = c_{x_o} H$$

$$\Psi(-\infty, z) = c_{x_o} z \quad ; \quad \frac{\partial \Psi}{\partial x}(+\infty, z) = 0$$

$$\Psi(0^-, z) = \Psi(0^+, z) \quad ; \quad \frac{\partial \Psi}{\partial x}(0^-, z) = (0^+, z) \tag{29}$$

3. INVERSE COORDINATES AND LINERIZATION

Given the convective nature of several key quantities, the stream function Ψ is a natural independent variable for our problem. This will be particularly helpful for numerical solution, since the discontinuity at $\Psi = \Psi_{TIP}$ can then be explicitly retained with no numerical smearing. We therefore change independent variables from (x,z) to (x,Ψ), and regard z as the new dependent quantity; the funtion $z(x,\Psi)$, of course, represents the shape of the streamlines. Using subscripts on z to denote differentiation, the velocity components are then

$$c_x = \frac{1}{z_\Psi} \quad , \quad c_z = \frac{z_x}{z_\Psi} \tag{30 a,b}$$

and also

$$\left(\frac{\partial c_x}{\partial z}\right)_{x=0} = -\left(\frac{z_{\Psi\Psi}}{z_\Psi^3}\right)_{x=0} \tag{31}$$

and the Laplacian operator becomes

$$\nabla^2\Psi = \frac{1}{z_\Psi^3}\left[-z_\Psi^2 z_{xx} + 2 z_x z_\Psi z_{x\Psi} - (1 + z_x^2) z_{\Psi\Psi}\right] \tag{32}$$

The governing equation $\nabla^2\Psi = \omega_y(\Psi)$, which in its original form was nonlinear by virtue of the dependence of ω_y on Ψ, is now non-linear only because of the derivative products on its left-hand side. Whereas linearization in the original coordinates would imply regarding ω_y as a small quantity, linearization in inverse coordinates can fully retain ω_y, and implies only neglecting certain products of velocity disturbances on the LHS of the equation. Thus, although the results will be later verified by numerical solution of the full non-linear equation, we begin our investigation by linearizing $z(x,\Psi)$ about the uniform flow condition:

$$z = \frac{\Psi}{c_{x_0}} + \tilde{z} \tag{33}$$

where c_{x_0} is the velocity far upstream of the disk, and $\tilde{z} << z$.

For the velocity components this implies, to first order,

$$c_x \cong c_{x_0} - c_{x_0}^2 \tilde{z}_\Psi$$
$$c_z \cong c_{x_0} \tilde{z}_x \tag{34a,b}$$

The governing equation (Eq. (28)) reduces, to first order, to:

$$\text{UPSTREAM: } \frac{1}{c_{x_0}^2} \tilde{z}_{xx} + \tilde{z}_{\psi\psi} = 0$$
$$\text{DOWNSTREAM } \left\{ \begin{matrix} \text{GAP} \\ \text{BLADES} \end{matrix} \right\}: \tag{35}$$

$$\frac{1}{c_{x_0}^2} \tilde{z}_{xx} + \tilde{z}_{\psi\psi} = - \left\{ \frac{\tan^2 \alpha_2}{\frac{U}{(c_x)_{x=0}} \tan \alpha_2 + \tan^2 \beta_3} \right\} (\tilde{z}_{\psi\psi})_{x=0} - \frac{Q}{c_{x_0}^2} \delta(\Psi, \Psi_{TIP}) \tag{35b}$$

and the boundary conditions are now

$$\tilde{z}(x,0) = \tilde{z}(x, c_{x_0} H) = 0 \tag{36a}$$
$$\tilde{z}(-\infty, \Psi) = \tilde{z}_x(+\infty, \Psi) = 0 \tag{36b}$$
$$\tilde{z}(0^-, \Psi) = \tilde{z}(0^+, \Psi) \tag{36,c}$$
$$\tilde{z}_x(0^-, \Psi) = \tilde{z}_x(0^+, \Psi) \tag{36,d}$$

The shear layer strength Q in Eq. (35b) remains as defined by Eq. (27), where c_x^+ and c_x^- are to be found as part of the solution.

4. The Nature of the Throughflow Distributiuon at the Disk

Although there is some interest in the flow distributions elsewhere, the main results to the obtained depend on how the flow is distributed at the disk itself. We will show in this section that, in the present linearized approximation, the distribution consists of two constant, but different axial velocity levels; one for flow crossing the gap, and one for flow through the bladed region.

One part of the proof relies on a general property of linearized actuator disk flow; the disturbance at the disk is half as strong as it is

far downstream. This property is best known from elementary propeller theory, where it holds (with no need for linearization) by virtue of the constancy of the background pressure. For linearized, confined flows, it is proven, for example, in Horlock's monograph[11]. Since Horlock's analysis is in direct coordinates, the statement must be qualified by saying that the disturbance doubles between disk and downstream stations at the same z coordinate. In our analysis i.e., with (x, Ψ) as coordinates, the disturbances double along a given streamline. A proof is given in Appendix A. The "disturbance" can be either $\tilde{z}(\Psi)$, the displacement of a streamline, or $\frac{d\tilde{z}}{dx}$, its slope. Using the latter form, then,

$$\left(\frac{\partial \tilde{z}}{\partial x}\right)_{x=\infty} = 2\left(\frac{\partial \tilde{z}}{\partial x}\right)_{x=0} \text{ (same } \Psi) \tag{37}$$

or, using Eq. (34a),

$$\left(\frac{\partial c_x}{\partial z}\right)_{x=\infty} = 2\left(\frac{\partial c_x}{\partial z}\right)_{x=0} \tag{38}$$

On the other hand, the shear $\left(\frac{\partial c_x}{\partial z}\right)_{x=\infty}$ far downstream equals the corresponding vorticity $(\omega_y)_{x=\infty}$, which is given, for example, by the right-hand side of Eq. (35b), times $-c_{x_o}^3$. Excluding the concentrated vorticity Q at $\Psi = \Psi_{TIP}$, and using Eq. (31), this takes the form

$$\left(\frac{\partial c_x}{\partial z}\right)_{x=\infty,\Psi} = \omega_y(\Psi) = F(\Psi)\left(\frac{\partial c_x}{\partial z}\right)_{x=o} \tag{39}$$

where $F(\psi) \equiv -\left\{ \frac{\tan^2 \alpha_2}{\frac{U}{(c_x)_{x=o}} \tan \alpha_2 + \tan^2 \beta_3} \right\}$ $\left(\left\{ \begin{matrix} \text{GAP} \\ \text{BLADES} \end{matrix} \right\} \right)$ (40)

Comparing Eqs. (38) and (39), we can see that, both shears, $\left(\frac{\partial c_x}{\partial z}\right)_{x=0}$ and

$\left(\frac{\partial c_x}{\partial z}\right)_{x=\infty}$ must be zero, unless $F(\Psi) = 2$. This latter condition is ruled out by Eq. (40), which shows $F(\Psi) \leq 0$. Once again, this excludes the vorticity concentration at $\Psi = \Psi_{TIP}$.

We can therefore conclude that the axial velocity distribution at the disk must have the piecewise constant form shown schematically in Fig. 5. Since the work done by the flow is uniquely related to the disk throughflow $(c_x)_{x=0}$ (see Eqs. (23), (24)), the implication is that the turbine work defect due to the presence of the gap will be distributed uniformly along the blade span, in correspondence with the uniform decrease of $(c_x)_{x=0}$. This is at first sight counter-intuitive, given the strong localized effects produced by the gap flow (leakage jets, rolled-up structures, etc). Indeed, the non-linear solutions reported later (Sec 7.) show some amount of extra work defect near the tip, but the main component by far still reamins distributed. This effect may be thought of as the result of the transverse pressure forces set up in the confined flow by the presence of the gap. These forces ensure that the extra flow going to from the gap jet is evenly supplied by the whole passage, and it is this small flow defect that is responsible for the work defect. On the other hand, it remains true that strong total pressure losses must be associated with the dissipation of the sharp discontinuities created near the tip, and this must be taken into account as well when calculating the effect of the tip gap on turbine efficiency (See Sec. 5.2).

5. Solution of the Linearized Equations

5.1 Disk Quantites

Since $c_x(x = o)$ is piecewise constant, the distributed part of the forcing term in Eq. (35b) disappears, leaving only the shear layer:

$$\frac{1}{c_{x_0}^2}\tilde{z}_{xx} + \tilde{z}_{\psi\psi} = -\frac{Q}{c_{x_0}^2}\delta(\Psi - \Psi_{TIP}) \quad (x > 0) \tag{41}$$

The values of the two disk velocity levels (Figs. 5) can be obtained as follows. First, since $(\omega_y)_\infty = -c_{x_o}^3(\tilde{Z}_{\psi\psi})_\infty$ (the x-derivatives

vanish), then, integrating across the shear layer at $x = \infty$, and using the definition of Q (Eq. 26),

$$\left(\tilde{Z}_\Psi^+ - \tilde{Z}_\Psi^-\right)_{x=\infty} = -\frac{Q}{c_{x_0}^3} \tag{42}$$

where the superscripts $(^+)$ and $(^-)$ refer to the jet and blades side of the layer, respectively. At the disk, the difference of the $\tilde{Z}_\Psi$ values must then be $\frac{1}{2}$ as much:

$$\left(\tilde{Z}_\Psi^+ - \tilde{Z}_\Psi^-\right)_{x=0} = -\frac{Q}{2\,c_{x_0}^3} \tag{43}$$

Also, flow continuity $\left(\tilde{Z}(0,0) = \tilde{Z}(0, Hc_{x_0}) = 0\right)$ plus the constancy of both $\tilde{Z}_\Psi^+$ and $\tilde{Z}_\Psi^-$, can be expressed as

$$\lambda\left(\tilde{Z}_\Psi^+\right)_{x=0^+} + (1-\lambda)\left(\tilde{Z}_\Psi^-\right)_{x=0} = 0 \tag{44}$$

where λ is the fractional flow through the gap (namely, $\Psi_T = (1-\lambda)\,Hc_{x_0}$.) The quantity λ is regarded as a given in our formulation, while the geometrical gap width, δ, is not.

Solving Eqs. (43) and (44) together,

$$\left(\tilde{Z}_\Psi^+\right)_{x=0} = -\frac{1-\lambda}{2\,c_{x_0}^3}Q$$

$$\left(\tilde{Z}_\Psi^-\right)_{x=0} = \frac{\lambda}{2\,c_{x_0}^3}Q \tag{45a,b}$$

which translates into the axial velocities (see. Eq. 34)

$$\frac{c_x}{c_{x_0}} = \begin{cases} 1 + \dfrac{Q}{2\,c_{x_0}^2}(1-\lambda) & \text{.....(GAP)} \\ 1 - \dfrac{Q}{2\,c_{x_0}^2}\lambda & \text{.....(BLADES)} \end{cases} \tag{46a,b}$$

Since this gives us the velocities c_x^+ and c_x^- at the disk, we can now substitute (46a,b) into the definition (Eq. (27)) of Q, which yields a quadratic equation for Q as a function of λ.

After some rearrangement, this is

$$\frac{(1-\lambda)^2 \tan^2 \alpha_2 - \lambda^2 \tan^2 \beta_3}{4} q^2 + \left[2 + (1-\lambda)\tan^2 \alpha_2 + \frac{\lambda}{\phi} \tan \alpha_2 + \lambda \tan^2 \beta_3\right] q -$$

$$\left[\frac{2}{\phi} \tan \alpha_2 - \frac{1}{\phi^2} + \tan^2 \beta_3 - \tan^2 \alpha_2\right] = 0 \qquad (47)$$

where ϕ is the flow coefficient

$$\phi \equiv \frac{Cx_0}{U} \qquad (48)$$

and the dimensionless shear layer strength is $q = \frac{Q}{c_{x_0}^2}$ (49)

The implied gap width, δ, can be easily calculated. Integrating Eq. (45b) from $\Psi = 0$ to $\Psi = \Psi_{TIP} = (1 - \lambda)\, Hc_{x_0}$

$$\frac{\tilde{Z}_{TIP}}{H} = \lambda\,(1-\lambda)\,\frac{q}{2} \qquad (50)$$

Adding to this he undisturbed value ($(1-\lambda)$ H), we obtain Z_{TIP}, and then $\delta = H - Z_{TIP}$. The result is

$$\frac{\delta}{H} = \lambda\left[1 - (1-\lambda)\frac{q}{2}\right] \qquad (51)$$

This can also be solved for the leakage if the gap is given:

$$\lambda = \frac{2\,(\delta/H)}{1 - \frac{q}{2} + \sqrt{\left(1 - \frac{q}{2}\right)^2 + 4\left(\frac{\delta}{H}\right)\left(\frac{q}{2}\right)}} \qquad (52)$$

Notice that λ depends non-linearly on (δ/H), both explicity, and through the dependence of q on λ (Eq. (47)). For the practical, small values of λ and (δ/H) this is not a strong non-linearity, however.

5.2 Work Defect and Efficiency Losses

The power extracted by the turbine, and hence the tip loss coefficient, can also be calculated easily. In coefficient form,

$$\psi \equiv \frac{1}{\dot{m}U^2} \int_0^{\Psi_{TIP}} (h_{t_1} - h_{t_3})\, \rho d\psi \tag{53}$$

The total enthalpy drop is given by Eq. (21) for the bladed area (using $c_x = \bar{c_x}$), and is zero for the gap.

Remembering that $\rho \frac{\Psi_{TIP}}{\dot{m}} \equiv 1 - \lambda$, we obtain

$$\Psi = (1 - \lambda)\left[\phi\,(\tan\alpha_2 + \tan\beta_3) - 1 - \lambda\,\phi\,\frac{q}{2}\,(\tan\alpha_2 + \tan\beta_3)\right]$$

For zero leakage, $\Psi_o = \phi\,(\tan\alpha_2 + \tan\beta_3) - 1$. The relative work defect is then

$$\frac{\psi_o - \psi}{\psi_o} = \lambda\left[1 + \frac{\psi_o + 1}{\psi_o}\,\frac{1 - \lambda}{2}\,q\right] \tag{54}$$

We can now calculate a work defect coefficient w as the relative work decrease (Eq. 54) divided by the relative gap width, δ/H. Using Eq. (51),

$$w = \frac{1 + \frac{\psi_o + 1}{\psi_o}\,\frac{1 - \lambda}{2}\,q}{1 - \frac{1 - \lambda}{2}\,q} \tag{55}$$

This coefficient is not to be confused with the efficiency-loss coefficient β introduced earlier (Eqs. 1-4). If we agree to work with the total-to-total efficiency η, its evaluation requires in addition the calculation of the total pressure $(P_t)_{MIX}$ at a hypothetical downstream section where the shear layer has dissipated and conditions are again uniform.

At this "mixed-out" downstream station, the axial velocity must again be c_{x_o} (to conserve mass) and the tangential velocity (from y-momentum balance) must be

$$c_{y_{MIX}} = \lambda\, c_y^+ + (1 - \lambda)\, c_y^- \tag{56}$$

where c_y^+ and c_y^- are the tangential velocities in the fluid above and below the shear layer, respectively. Prior to mixing, both c_y^+ and c_y^- are uniform in their respective domains, because they are uniform at the disk (in our two-level approximation), and are then purely convected from there. From Fig. 4 we have

$$c_y^+ = c_x^+ \tan \alpha_2 \tag{57}$$

$$c_y^- = U - c_x^- \tan \beta_3 \tag{58}$$

where Eq. (57) reflects the assumption of zero turning of the gap flow, and (58) assumes perfect guidance by the rotor blades for the rest of the flow.

The total pressure in the mixed-out region is given by

$$\frac{P_{t_o} - P_{t_{MIX}}}{\rho} = \frac{P_o - P_\infty}{\rho} - \frac{1}{2} c_{y_{MIX}}^2 \tag{59}$$

where P_∞ is at a far downstream position, (before or after mixing) and we have taken advantage of $(c_x)_\infty = c_{x_0}$, $(c_z)_\infty = 0$. The static pressure drop can be calculated for a streamline which goes through the blades. The drop $P_1 - P_3$ <u>at the disk</u>, is given in Eq. (23). Upstream of the disk,

$$\frac{P_o - P_1}{\rho} = \frac{1}{2}\left(c_x^{-2}\right)_{x=o} - \frac{1}{2} c_{x_o}^2 \tag{60}$$

and downstream, since c_y^- remains invariant,

$$\frac{P_\infty - P_3}{\rho} = \frac{1}{2}\left(c_x^{-2} + c_z^2\right)_{x=o} - \frac{1}{2}\left(c_x^{-2}\right)_\infty \tag{61}$$

Here $c_z^2\,(x = 0)$ is a 2nd order quantity in our linear analysis, and will be ignored. Substracting (60) and (61),

$$\frac{P_o - P_\infty}{\rho} = \frac{P_1 - P_3}{\rho} + \frac{1}{2}(\bar{c_{x_\infty}})^2 - \frac{1}{2}\, c_{x_o}^2 \tag{62}$$

Combination of Eqs. (58), (61) and (23) therefore gives the total pressure from far upstream to the hypothetical downstream mixed-out station. This quantity is the ideal work extracted per unit volume, and the efficiency is then

$$\eta = \frac{\Psi}{\left(\frac{P_{t_o} - P_{t_{MIX}}}{\rho U^2}\right)} \tag{63}$$

where Ψ is as given by Eq. (54). The efficiency loss factor follows as

$$\beta = \frac{1 - \eta}{\delta/H} \tag{64}$$

As noted, the efficiency η is affected by the decrease of Ψ due to the gap, but (see Eq. 62) also by that of the total pressure drop. With no gap, and everything else being ideal, we would have $\eta = 1$. Let the total pressure drop be therefore expressed as

$$\frac{P_{t_o} - P_{t_{MIX}}}{\rho U^2} = \psi_o\,(1 - \xi) \tag{65}$$

where ξ (which is a positive quantity) can be calculated following the outline explained above. Then it is easy to show that the loss factor β and the work defect factor w are related through

$$\beta = \frac{w - \xi}{1 - \xi \frac{\delta}{H}} \tag{66}$$

so that β is in general smaller than w. Calculated results will be shown in Section 6.

5.3 Velocity Distribution away from Disk

The solution to Eq. (41) is most easily written in terms of Fourier series in Ψ, which can also represent the discontinuities occurring along the shear layer. This is the form naturally obtained by formal separation of variables. Imposing all the boundary conditions listed by Eq. (29), we obtain

$$\frac{\tilde{z}}{H} = \begin{cases} \sum_{n=1}^{\infty} \alpha_n e^{\frac{n\pi x}{H}} \sin n\pi\theta & (x < 0) \\ \sum_{n=1}^{\infty} \alpha_n \left(2 - e^{-\frac{n\pi x}{H}}\right) \sin n\pi\theta & (x > 0) \end{cases} \tag{67}$$

where

$$\theta \equiv \frac{\Psi}{Hc_{x_o}} \tag{68}$$

and the α_n coefficients are yet to be found.

The Ψ- derivative at the disk is

$$(\tilde{z}_\Psi)_{x=o} = \frac{\pi}{c_{x_o}} \sum_{n=1}^{\infty} n\alpha_n \cos n\pi\theta \tag{69}$$

This must be identified with the distribution of $\tilde{z}_\Psi$ given by Eqs. (45), i.e. $\tilde{z}^-_\Psi$ for $0 < \theta < 1 - \lambda$ and $\tilde{z}^+_\Psi$ for $1 - \lambda < \theta < 1$. Fourier inversion then yields

$$\alpha_n = \frac{Q}{\pi^2 c_{x_o}^2} (-1)^{n+1} \frac{\sin n\pi\lambda}{n^2} \tag{70}$$

When these α_n's are substituted back into Eq. (66), the resulting infinite series are in general not summable in closed form. However, the derivatives of $\tilde{z}$, which are related to velocity perturbations (Eq 34), can indeed be summed. Without stopping to discuss the details (see Ref. 12) the results take the following forms:

UPSTREAM:

$$\frac{c_x}{c_{x_o}} = 1 - \frac{Q}{2\pi c_{x_o}^2}\left\{\tan^{-1}\left[\frac{\sin\pi(1-\theta-\lambda)}{e^{-\pi x/H} - \cos\pi(1-\theta-\lambda)}\right] - \tan^{-1}\left[\frac{\sin\pi(1-\theta+\lambda)}{e^{-\pi x/H} - \cos\pi(1-\theta+\lambda)}\right]\right\}$$

$$\frac{c_z}{c_{x_o}} = \frac{Q}{4\pi c_{x_o}^2}\ln\left[\frac{1 - 2\,e^{\pi x/H}\cos\pi(1-\theta+\lambda) + e^{2\pi x/H}}{1 - 2\,e^{\pi x/H}\cos\pi(1-\theta-\lambda) + e^{2\pi x/H}}\right]$$

(70a,b)

DOWNSTREAM $\begin{pmatrix}\text{GAP}\\ \text{BLADES}\end{pmatrix}$

$$\frac{c_x}{c_{x_o}} = 1 - \frac{Q}{2\pi c_{x_o}^2}\left\{\begin{pmatrix}-2\pi(1-\lambda)\\ 2\pi\lambda\end{pmatrix} + \tan^{-1}\left[\frac{\sin\pi(1-\theta-\lambda)}{e^{\pi x/H} - \cos\pi(1-\theta-\lambda)}\right] + \tan^{-1}\left[\frac{\sin\pi(1-\theta+\lambda)}{e^{\pi x/H} - \cos\pi(1-\theta+\lambda)}\right]\right\}$$

$$\frac{c_z}{c_{x_o}} = \frac{Q}{4\pi c_{x_o}^2}\ln\left[\frac{1 - 2\,e^{-\pi x/H}\cos\pi(1-\theta+\lambda) + e^{-2\pi x/H}}{1 - 2\,e^{-\pi x/H}\cos\pi(1-\theta-\lambda) + e^{-2\pi x/H}}\right]$$

(71a,b)

The c_x discontinuity is apparent (Eq. 71a). The expressions also show clearly that the axial scale of the near-disk potential effects is H/π, which, while being probably many times the gap width δ, is still likely to be small compared to the mean radius R of the stage. This fact can be exploited in studying the effects of azimuthal variations of gap width.

Particularization of Eqs. (70a) and (71a), for x = o do yield the known two-level velocity distribution (Eq. 46). On the other hand, Eqs. (70b) or (71b) give the spanwise flow velocity at the disk as

$$\left(\frac{c_z}{c_{x_o}}\right)_{x=o} = \frac{Q}{2\pi\, c_{x_o}^2}\ln\frac{\sin\frac{\pi}{2}(1-\theta+\lambda)}{\sin\frac{\pi}{2}(1-\theta-\lambda)} \qquad (72)$$

which exhibits a logarithmic singularity at the tip $(\theta = 1 - \lambda)$.

The shape of the streamline which supports the shear layer is of some interest. Putting $\theta = 1 - \lambda$ in Eq. (71b) and relating $\tilde{c}_z$ to $\tilde{z}_x$ by Eq. (34b) gives

$$\frac{d\tilde{z}}{dx}(\psi_{TIP}, x) = \frac{Q}{4\pi c_{x_o}^2} \ln\left[1 + 4 \sin^2 \pi\lambda \frac{e^{-\pi x/H}}{\left(1 - e^{-\pi x/H}\right)^2}\right] \tag{73}$$

This is not analytically integrable, but for small λ, and provided $\frac{x}{H} >> \lambda$ (which only excludes the immedicate vicinity of the gap), we can expand the logarithm in (73), and then integrate with the condition

$$\frac{\tilde{z}}{H}(\psi_{TIP}, \infty) = 2\frac{\tilde{z}}{H}(\psi_{TIP}, 0) = 2\left(\lambda - \frac{\delta}{H}\right) \tag{74}$$

Including the unperturbed contribution $(1 - \lambda)$, this gives

$$\frac{\tilde{z}}{H}(\psi_{TIP}, x) \cong 1 - \lambda + Q\left\{\lambda(1-\lambda) + \left(\frac{\sin \pi\lambda}{\pi}\right)^2\left[1 - \frac{1}{\left(1 - e^{-\frac{\pi x}{H}}\right)^2}\right]\right\} \tag{75}$$

6. Some Results of the Linearized Model

6.1 Parametric Trends

This subsection gives some simple calculated results from the formulae obtained so far, in order to illustrate the trends and sensitivities involved. Further results and comparisons to data are deferred to Secs. 6.2 and 9.2.

As might be expected, the degree to reaction R (see Appendix B for definitions used) is an important parameter controlling the effects of tip leakage. At very high R the turbine is lightly loaded and the effect of the gap is small. This can be seen most easily in the zero exit swirl case, when Eqs. (B4) and (B7) indicate $\psi = 2(1 - R)$, so that $\psi \to 0$ when $R \to 1$. At the other, and more realistic end (small R), the individual turbine blades are highly loaded, but there is little net pressure drop across the rotor. Since there is then little incentive for approaching flow to migrate spanwise towards the gap region, little blade unloading is expected. Thus, the shear strength Q and the loss

parameter β are expected to show maximum values at some intermediate degree of reaction, For the same reasons, the difference between the relative gap δ/H and relative leakage rate, λ, will also peak at that intermediate R.

These trends are shown in Figs. 6 and 7. Here the leakage λ was held at 0.1 and the degree of reaction R was varied over the range 0-1, while the flow coefficient ϕ was given values from 0.3 to 0.7. Zero exit swirl was assumed, and so different ϕ values imply different turbine angles β_3, while varying R amounts to varying the stator blade angle α_2. The expected peak in loss factor is seen to occur for $R \cong 0.8$, which is higher than the practical range for turbines (0 - 0.6 or so). Hence, in practice, the expected trend would be for losses to increase with degree of reaction. This trend is clearly exhibited in Waterman's data compilation[3], as indicated in Fig. 8 (taken fom Ref. 3). More detailed data analysis will be shown in Secs. 6.2 and 9.2. The minimum of δ/H at $R \cong 0.8$ shown in Fig. 7 confirms that redistribution effects are indeed strongest then, since the smallest gaps is required to pass a given leakage.

So far parametric results ("rubber engine") have been discussed. For a given turbine (given α_2, β_3) some trends are shown in Figs. 9 and 10. Fig. 9 shows the two axial velocity levels at the disk as the gap only is varied (as reflected in the leakage rate). While both velocities vary only slightly with gap, it must be remembered that for the bladed region, it is the difference $1 - \frac{c_x}{c_{x_o}}$ that controls the losses, and this difference does have a substantial variation. On the other hand, the "jet" velocity changes are not particularly significant, as one would expect, since they mostly respond to the fixed ΔP across the turbine. Of course the word "jet" must be used with caution, since only the x-component of the velocity is shown.

In Fig. 10 all geometrical parameters, including gap size, are fixed and the flow coefficient is varied. This allows non-zero exit swirl to occur (ranging from $c_{\overline{y}_3}/c_{x_o} \cong 0.73$ at $\phi = 0.27$ to $c_{\overline{y}_3}/c_{x_o} \cong -0.47$. at

ϕ = 0.4, with zero exit swirl at ϕ = 1/3). As the flow varies, the degree of reaction remains approximately fixed (close to the design value of 0.5), but turbine loading Ψ_o increases with ϕ, as shown in the lower scale. As the results show, the tip leakage fraction remains at about 1.5 times the relative gap throughout. On the other hand, the loss factor β increases strongly with flow, and weakly with decreasing gap.

6.2 Comparison to Turbine Data

We can now compare the calculated losses to those reported in the experimental literature. We rely for this on the compilation of Ref. 3, which gives data for ten cases (nine different turbines) over a wide range of parameters. Ref. 3 reports for each case the tip values of the work co-efficient Ψ_o (two definitions), degree of reactor R, flow coefficient ϕ, and individual blade loading (lift coefficient c_L, based in inlet relative velocity and blade area, and Zweifel coefficient (tangential force coefficient based on tangential area and exit dynamic head). Also reported are the relative gap and, in some instances, other geometrical parameters. As noted in the Introduction, Ref. 3 also shows the results of several existing loss correlations or theories when applied to these cases, plus the actual measured loss factor β.

One potential difficulty in application is that only tip parameters are given, whereas from the nature of our theory we suspect that mean parameters might be more appropriate.

Starting from Ψ_o (with the definition which agrees with that in our Appendix B), ϕ and R, the equations in Appendix B allow calculation of the blade angles α_2, β_3. The fractional leakage, λ, is determined from the relative gap δ/H using Eq. 51. This involves the shear strength q, which itself depends somewhat on λ, so some iteration must be used. The remainder of the calculations is straightforward. Table 2 summarizes the results

Scanning Table 2 we first notice a large disagreenment for Case 1 (Kofskey turbine). This is an impulse rocket turbopump stage with extremely large reported tip loading (Ψ = 7.0). As the table shows, this leads to very large exit swirl ($c_{\bar{y}}/c_{x_o}$= - 3.2). No reasonable modification of the theory could be found to resolve the disagreement of the β calculated and that reported, which, as expected for a low-reaction stage, is low (β = 1.02). A calculation was made, as shown in the second from-last-row of table 2, with a load Ψ_o reduced to 2.0, which leads to near-axial exit flow, and this does predict β = 0.97, close to the measured value. This might indicate a large radial load gradient for this turbine, but this has not been investigated futher.

Excluding Case 1, the mean squared error in the predicted β is

$$\overline{\varepsilon^2} = \frac{1}{N}\sum_{N}(\beta_{DATA} - \beta_{CALC})^2 = 0.1434$$

This compares favorably with the results of applying the correlations of Kofskey, Ainley, Soderberg and Roelke (See Table 1). The mean error is $\bar{\varepsilon} = \frac{1}{N}\sum_{N}(\beta_{DATA} - \beta_{CALC})^2 = 0.1434$

which idicates a general under-prediction of the losses. The standard deviation is

$$\sigma = \sqrt{\varepsilon^2 - (\bar{\varepsilon})^2} = 0.337$$

7. Numerical Verification

The linearized solution has yielded important results, some of which defy our expectations. It is therefore important at this point to investigate the extent to which these results may have been compromised by the linearization. To this end, we need to solve by a numerical technique the complete non-liner actuator disk problem (Eqs. 28, 29). Inverse coordinates are still a convenient formulation, especially in that they fix the location of the shear layer along a coordinate line

($\Psi = \Psi_{TIP}$, $x > o$), thus avoiding the smearing inherent in any discontinuity-capturing approach that could be used in direct (x,z) coordinates. Simple finite differences on a rectangular grid can also be used effectively with such a formulation, since the main surfaces (disk, walls, shear layer) are all aligned with the coordinate lines (x,Ψ). The only disadvantage is the more complex form of the Laplacian in these coordinates (see Eq. 32).

The method used is a form of over-relaxation, which can be constructed starting from a minimum principle for the problem (See Ref. 12 for details). Care is taken to include the δ functon on the right-hand side of Eq. (28) in a consistent manner. Integrating Eq. (28) across the shear layer, and, as before, using superscripts (+) and (-) for the gap and bladed sides, respectively, one obtains at each x

$$\left(1 + z_x^2\right)\left[\frac{1}{\left(z_\Psi^+\right)^2} - \frac{1}{\left(z_\Psi^-\right)^2}\right] = 2\,Q \qquad (76)$$

where Q is calculated from disk vewlocities according to Eq. (27). In discretizing the connecting condition (76), one-sided differences are used for z_Ψ^+ and z_Ψ^- to avoid numerical "mixing" of the two streams. Most of the calculations were done on a 16 x 32 grid. As a check, one case was computed on a 24 x 48 grid, and the discrepancies (Table 3) were found to be below 10^{-3} in relative terms.

A series of numerical results showing the two velocity components at the disk, with the linearized theory results superimposed, are given in Figs 11 through 26. For degrees of reaction below 0.4 or above 0.90 the agreement is excellent. As expected, the worst linerarization errors occur in the vicinity of $R \cong 0.8$, but even then the results of the linear theory are found to be fairly accurate. Most importantly, the prediction that the axial velocity at the disk is piecewise constant is clearly borne out by the nonlinear results. The only noticeable deviation from throughflow uniformity in the bladed region occurs very near the blade tip (on the scale of the gap size), and its integrated effect is in any case minimal.

8. Partial Blade-Tip Loading

8.1 Introduction

One of the basic approximations made in the theoretical treatment so far is that of zero work done by any fluid crossing the gap area. If we include under that description any streamline which passes over one blade tip, this is clearly not an accurate assumption. Fig. 27, for example, shows that, prior to crossing over, a streamtube is partially deflected by the blade, and hence does some push work on it. The magnitude of this work could be quantified if the flow angle for the leakage fluid leaving the passages were known, which prompts us to a more detailed examination of the flow field around the blade-tip gap region.

The blade-tip region has been theoretically treated using a variety of approaches. The simple model of Rains[4], which is most appropriate for thin, lightly loaded blades, uses ideal, pressure-driven flow concepts to derive the speed and direction of the gap "jet". Even for the case of the thicker turbine blading, ideal flow is a fairly good approximation. For example, Rains[4] gave a criterion for viscous forces to be negligible, in the form

$$A \equiv \left(\frac{\text{GAP}}{\text{THICKNESS}}\right)^2 \times \left(\frac{\text{THICKNESS}}{\text{CHORD}}\right) \times R_e\,(\text{CHORD, REL. INLET, VELOCITY}) > 125 \tag{78}$$

For the experimental turbine being tested as part of our research on Alford forces, this parameter is approximately 1000, and this situation is quite common. On the other hand, the effects of chordwise pressure gradients on thick-blade tip flows, as well as that of relative wall motion are still potentially significant, and have not been treated so far.

The gap jet is known to interact strongly with the passage flow and to roll itself up into a concentrated vortex-like structure. Rains

himself derived [4] a semi-empirical expression for the trajectory of that vortex. Lakshminarayana [6,7] also used empirical information on the tip vortex location and strength to predict details of the blade pressure distribution, In fact, the strength of the vortex was explicitly related to a "partial blade-tip loading parameter", K, varying from 0 to 1, and inferred from extrapolation of surface pressure measurements near the tip to the end wall. Since there are very sharp pressure gradients in the pressure side of the blade, near the gap, this procedure is fraught with difficulties. More recently, G.T. Chen et al [13] have used vorticity dynamics to simulate the roll-up process, and have been able to predict accurately the trajectory of the vortex.

In what follows, we will introduce an alternative viewpoint which leads to simple, but accurate expressions for the location and size of the leakage vortex. This can then be used in calculating the flow leaving angle of, and hence the work done by the leakage flow.

8.2 Collision of the Leakage Jet and the Passage Flow

Fig. 28 shows schematically the essential features of the leakage flow. The fluid approaches a blade (here represented as a flat plate) with a relative velocity $\vec{w}_2$, which evolves into the passage flow velocity $\vec{w}_{PASS}$ at locations not very near the tip gap. Under the action of the pressure differential across the blade, a jet of leakage flow at velocity $\vec{w}_{jet}$ escapes under the blade. This jet penetrates a certain distance into the passage, but is eventually stopped by the main flow, which separates the jet from the wall, turns it backwards, and leads to the formation of a rolled-up structure containing both, leakage and passage fluid. This "collision" of the two streams is again shown in Fig. 29 in plan form, and Fig. 30 shows a schematic of the flow structure seen in a cut such as a-a in Fig. 29, with leakage fluid shown dashed.

Consider the situation at points along the jet separation line, such as P in Figs. 29,30. Ignoring frictional effects, the two streams which meet there (jet and passage flows) can both be traced back along different paths, to the inlet flow, and hence have equal total pressures and temperatures. Since they also have equal static pressures along their contact line, (and generally similar static pressures throughout

the region), these two streams must have equal velocity magnitudes. If the section a-a is perpendicular to OP, we can think of pont P (Fig. 30) as the common stagnation point of the two "colliding" flows, approaching each other with equal velocities, which are each the component of $\vec{w}_{jet}$ and $\vec{w}_{PASS}$ perpendicular to line OP. It follows that line OP must bisect the angle made by $\vec{w}_{jet}$ and $\vec{w}_{PASS}$. This gives a first and important piece of information about the location of the rolled up structure, but, since this structure has a finite and increasing transverse dimension, it does not yet locate its center.

To continue our discussion, notice that the transverse momentum balance of a fluid element near point P requires that both transverse colliding flows must bring equal (and opposite) momentum fluxes to the rolled-up structure. Since the two velocities are equal, we find that equal mass flows must be entering the rolled-up structure from both fluids. In other words, the clear and dashed areas in Fig. 30 must occupy equal fractions of the total "vortex" cross section. Let δ_{JET} be the jet thickness, and $w_{\parallel}$, $w_{\perp}$ the common components along and across OP of the colliding streams. The rate of increase of the cross-section $A_{\perp}$ of the rolled structure along OP is then given by

$$w_{\parallel} \frac{dA_{\perp}}{ds} = 2\, w_{\perp}\, \delta_{JET} \tag{78}$$

or, callling $\theta = \tan^{-1} \frac{w_{\perp}}{w_{\parallel}}$, i.e., the angle made by the separation line OP and the blade itself,

$$\frac{dA_{\perp}}{ds} = 2\, \delta_{JET} \tan\theta \tag{79}$$

where s is measured along the vortex trajectory.

The precise shape of the rolled-up structure is more difficult to establish, but it seems reasonable to model it as (half) cylindrical ideal vortex in a cross-flow. Following Batchelor[14] such a vortex is describable by the stream function (Fig. 31)

$$\Psi = 1.298\, w_{\perp}\, R\, J_1\left(3.83 \frac{r}{R}\right) \sin\theta_1 \tag{80}$$

where R is the radius of the dividing streamline, $J_1(x)$ is the Bessel's function of the 1st order (with a zero at x = 3.83) and (r, θ_1) are polar coordinates. The vorticity in this flow is distributed inside the semi-circle of radius R in proportion to Ψ:

$$\omega = \left(\frac{3.83}{R}\right)^2 \Psi \tag{81}$$

and is zero outside. Integration of ω gives an overall circulation

$$\Gamma = 6.83\, w_\perp R \tag{82}$$

whereas integration of $r \sin\theta\, \omega$ gives a center of vorticity height of

$$z_c = 0.460\, R \tag{83}$$

We thus make $A_\perp = \frac{1}{2}\pi R^2$, and measuring distance along the blade $(x_{BL} = s \cos\theta)$, we can integrate Eq. (79) to obtain

$$R = \sqrt{\frac{4}{\pi}\left(\frac{\tan\theta}{\cos\theta}\right)\delta_{JET}\, x_{BL}} \tag{84a}$$

The trajectory of the vortex center then follows (Fig. 32) as

$$y_c = x_{BL} \tan\theta - \frac{R}{\cos\theta} \tag{84b}$$

To complete the analysis, the angle θ must now be determined. From our discussion of the separation line OP, this angle was shown to be half of the angle β between the blade and the jet flow:

$$\theta = \beta/2 \tag{85}$$

This angle β follows from the simple local analysis first proposed by Rains[4], which applies to thin blades when viscous effects can be neglected, In Fig. 33, w_p and w_s are the flow velocities on the pressure and suction sides of the blade, respectively. Application of Bernoulli's equation relates these velocities to the corresponding pressures:

$$w_p = \sqrt{w_2^2 - 2\frac{P_p - P_2}{\rho}} \tag{85}$$

$$w_s = \sqrt{w_2^2 + 2\frac{P_2 - P_s}{\rho}} \tag{86}$$

where P_2, w_2 corresponds to inlet conditions. On the other hand, the leakage jet emerges form the gap with a velocity component perpendicular to the blade of

$$w_G = \sqrt{2\,\frac{P_p - P_s}{\rho}} \tag{87}$$

and its components parallel to the blade is simply w_p, since no momentum is added or lost in that direction during passage throught the gap. It can be verified that the net magnitude w_{JET} of the jet velocity is then equal to w_s, as indicated previously. We then obtain (Fig. 33)

$$\tan\beta = \frac{w_G}{w_p} = \sqrt{\frac{(C_p)_p - (C_p)_s}{1 - (C_p)_p}} \tag{88}$$

where $c_p = 2((P-P_2))/\rho\, w_2^2$ in each case. Note that $(c_p)_p - (c_p)_s$ is the local lift coefficient c_L', referred to the relative turbine inlet velocity. Using the half-angle trigonometric formulae,

$$\tan\theta = \frac{\sqrt{(C_p)_p - (C_p)_s}}{\sqrt{1 - (C_p)_s} + \sqrt{1 - (C_p)_p}} \tag{89}$$

Notice that, as shown in Fig. 33, the vorticity vector corresponding to the shear between the jet and the adjacent passage flow is inclined at $\theta = \beta/2$ w.r.t. the blade, i.e. it is parallel to the outer edge OP of the rolled-up structure, This is also the direction of the mean flow between the two sides of the shear layer, which means that the shear vorticity is not convected at all towards the line OP. The only reason the vorticity Γ rolled up into the structure increases with downstream distance is that the growth of R gradually overlaps more and more of the shear vorticity. In this sense, the commonly invoked view of the rolled-up vortex growing by the connection of shed vortices must be used with caution.

Eqs. (84a), (84b) and (89) can now be used to calculate the vortex geometry if the suction and pressure side C_p distributions are know from experiments or calculations. A simple approximation can be obtained using the theory of lightly loaded thin wing profiles. In this approximation, $(w_p + w_s)/2 \cong w_2$, which when used in Eq. (85, (86) reduces both $(C_p)_p$ and $(C_p)_s$ to functions of $c_L' = (C_p)_p - (C_p)_s$ alone. Using this in Eq. (79) gives finally

$$\theta = \cos^{1} \begin{cases} \sqrt{\dfrac{4}{4 + c_L'}} & (c_L' < 4) \\ \sqrt{\dfrac{c_L'}{4 + c_L'}} & (c_L' > 4) \end{cases} \tag{90}$$

Notice the relative insensitively of θ to c_L', particularly about he common value $c_L' = 4$, when θ reaches a maximum of 45°.

8.3 Comparison to Vorticity Dynamics Model and to Data

Ref. (13) has recently provided a means of correlating a varitey of rolled-up vortrex data using a similarity analysis. Transverse distances are normalized by gap width δ, and axial distance, or time-of-flight are characterized by a parameter

$$t^* = \frac{x}{c_x \delta} \sqrt{\frac{\Delta P}{\rho}} \tag{91}$$

where x and c_x are axial distance and velocity and $\Delta P = P_p - P_s$. The data from many experiments (mainly from compressor cascades) correlate well with t^*. In addition, a calculational method was developed in Ref. 13 to track a series of shed tip vortices from an impulsively started plate, which represents the situation seen from a convective frame as the flow passes over a blade. The calculated results were shown to also correlate well with t^* and and with the data.

We use the correspondence

$$\frac{c_x}{w_2} = \cos \beta_2 \quad , \quad \frac{x}{x_{BL}} = \cos \beta_m \tag{92}$$

where β_2 and β_m represent the relative flow angles at the rotor inlet and on average in the rotor, respectively, to derive

$$\frac{x_{BL}}{\delta_{JET}} = \frac{\sqrt{2}}{\mu} \frac{w_2}{w_G} \frac{\cos \beta_2}{\cos \beta_m} t^* \tag{93}$$

where $\mu = \delta_{JET}/\delta$ is the gap discharge coefficient. Note also that $\frac{w_2}{w_G} = 1/\sqrt{c_L'}$.

For an approximate comparison, we use Rains' (4) values

$\mu = 0.785$ $\quad c_L' = 1.35$ $\quad \dfrac{\cos \beta_m}{\cos \beta_2} = 1.1$

to relate t^* to our x_{BL}, and then calculate the vortex trajectory using Eqs. (84a), (84b), (89) and (90). The results are compared in Fig. 34 to those reported in Ref. (13). The agreement with the data is satisfactory. Additional verification against the theory of Ref. (13) can be provided by comparing the predictions of both theories regarding the "center of vorticity" location in a cross-plant similar to that shown in Fig. 30. in order to be consistent with the calculations of Ref. (13), we have included here both, the rolled-up vorticity Γ (Eq. 83), and a vorticity $2w_\perp$ per unit length (perpendicular to $\vec{\omega}$) of the not-yet-rolled shear layer.

In calculating the distance z_c between the center of vorticity and the wall, we took this latter contribution to be at a distance δ_{JET}, and that of the rolled-up vortex to be at $\delta_{JET} + 0.46R$ (Eq. 82). The results are shown in Fig. 35, which again shows good agreement between our method and that of Ref. 13.

9. Blade-Tip Losses Including Partial Tip Loading

9.1. Modications of the Actuator-Disk Model

We now abandon the assumption of zero work done by the leakage fluid. This is somewhat less drastic a step then it might seem to be. Conceptually, we will now claim that the fluid which crosses the gap between the casing and a turbine blade is only partially underturned when compared to passage fluid. The fractional work done per unit mass of this leakage fluid will turn out to be about 50%, typically. On the other hand, this fluid "collides" with passage fluid and coalesces with it, leaving the rotor mainly in the form of a rolled-up vortex which includes 50% each, gap and passage fluid. Thus, an equivalent amount of passage fluid ends up being underturned as well. These two effects, partial under-turning of gap fluid, and partial under-turning of vortex-entrained passage fluid, tend to add up to the same net result as in the more idealized model considered so far.

There are three specific modifications to be made to the theory in order to incorporate these effects:

(a) Re-defining the"leakage flow fraction", λ, to include all under-turned fluid. Of this, only the fraction $\lambda/2$ is gap flow, and this is what must be related to the physical gap, δ (Eqs. 51 or 52).

(b) Allowing a non-zero total enthalpy drop for the gap flow, and relating it to the angle θ by which the flow fraction λ under-turns. This angle is supplied by a form of the theory of Sec. 8.

(c) Recognizing that the fluid comprising λ has not undergone an isentropic work-producing process, since formation of the rolled-up vortex is intrinsically lossy.

The under-turning angle θ should be calculated as an average which includes the rolled-up flow, assumed to have its momentum directed along the centerline of the rolled-up vortex, and also the portion of the gap jet which is not yet rolled up at exit (similar to the calculation described in Sec. 8.3 for the center of vorticity). In the interest of simplicity, we will take θ to be as given by Eq. (85), i.e., the angle between the blade and the outer edge of the vortex (Figs. 32, 33). This will to some extent cancel the modifications due to, on one hand, the angle between this outer edge and the vortex centerline, and, on the other hand, the contribution of the un-rolled jet, which is more strongly under-turned.

Let β_m be the average angle of the rotor blades to the axial direction which can be calculated (Fig. 4) as

$$\beta_m = \frac{\beta_3 - (\beta_2)_{DES.}}{2} \tag{94}$$

$$\text{with } \tan(\beta_2)_{DES} = \tan\alpha_2 - \frac{1}{\phi_{DES}} = \tan\alpha_2 - \tan\beta_3 \tag{95}$$

The passage flow relative velocity is then (on average) $w_{PASS} = \frac{c_x}{\cos\beta_m}$, which has components $w_{||}$ and $w_{\perp}$ parallel and perpendicular to the

line OP (Figs. 29, 30) which is now taken to represent the rolled-up vortex

$$w_{\parallel} = c_x \frac{\cos\theta}{\cos\beta_m} \quad ; \quad w_{\perp} = c_x \frac{\sin\theta}{\cos\beta_m} \tag{96}$$

The gap flow, for its part, has components $w_{\parallel}$ and $-w_{\perp}$ in the same directions. The flow fraction λ is all assumed to leave the passage with velocity $w_{\parallel}$ along line OP, and so its relative Y - component of velocity is $w_{11}\sin(\beta_m - \theta)$. In the absolute frame, then,

$$cy_3^+ = U - c_x^+ \frac{\cos\theta \sin(\beta_m - \theta)}{\cos\beta_m} \tag{98}$$

where we use the $^{(+)}$ superscript as before to denote the "gap fluid", which now, more precisely, means all of the under-turned fluid. Of course, the rest of the fluid has a $cy_3 = cy_3^-$ still given by Eq. (57). Also, the disk axial velocities c_x^+, c_x^- are still as given by Eqs. (46), although Q will now be different. Notice that Eq. (98) replaces the previously used non-turning assumption $(cy_3^+ = c_x \tan\alpha_2)$

Application of the Euler equation to both fluids gives the work done per unit mass by each stream:

$$W^+ = U\,(c_x^+ \tan\alpha_2 - cy_3^+)$$
$$W^- = U\,(c_x^- \tan\alpha_2 - cy_3^-) \tag{99a,b}$$

and, since ideality is assumed in the bladed region, ρW^- is the same asd the turbine total pressure drop in that region, i.e.

$$W^- = B_1 - B^- = B_1 - B_{\perp}^- - \frac{1}{2}(cy_3^-)^2 \tag{100}$$

In the "gap region", however, W^+ is less than the isentropic work $B_1 - B^+$ by an amount $T\Delta S$ equal the energy dissipation incurred in the mixing of the gap and passage streams. Per unit mass, this dissipation equals the kinetic energy associated with the "destroyed" component $w_{\perp}$ of Eq. (96):

$$T\Delta S = \frac{1}{2}\left(c_x^+ \frac{\sin\theta}{\cos\beta_m}\right)^2 \tag{101}$$

and therefore

$$W^+ = B_1 - B_\perp^+ - \frac{1}{2}(cy_3^+)^2 - \frac{1}{2}(c_x^+)^2\left(\frac{\sin\theta}{\cos\beta_m}\right)^2 \tag{102}$$

Subtracting Eqs. (100) and (102), and remembering that $Q = B_\perp^+ - B_\perp^-$, we obtain

$$Q = W^- - W^+ - \frac{1}{2}(c_X^+)^2\left(\frac{\sin\theta}{\cos\beta_m}\right)^2 - \frac{1}{2}(cy_3^+)^2 + \frac{1}{2}(cy_3^-)^2 \tag{103}$$

We can now use Eqs. (88) and (57) for the Cy's, and then Eq. (46) for the c_X's and, upon substitution into (102), we obtain the new equation for q. Rearranging this takes the form

$$\left[(1-\lambda)^2 G - \lambda^2\tan^2\beta_3\right]\left(\frac{q}{2}\right)^2 + 2\left[2 + \frac{\tan\alpha_2}{\phi} + (1-\lambda)G + \lambda\tan^2\beta_m\right]\left(\frac{q}{2}\right) - \left(\tan^2\beta_3 - G\right) = 0 \tag{104}$$

$$\text{where}\quad G = \left(\frac{\cos\theta\sin(\beta_m - \theta)}{\cos\beta_m}\right)^2 + \left(\frac{\sin\theta}{\cos\beta_m}\right)^2 \tag{105}$$

which replaces Eq. (47).

Once q is calculated, the total turbine work per unit mass is $\lambda W^+ + (1-\lambda)W^-$. Normalizing,

$$\psi = \psi_o - \lambda\phi(\tan\beta_3 - g)\left(1 + \frac{1-\lambda}{2}q\right) \tag{106}$$

$$\text{where}\quad g = \left(\frac{\cos\theta\sin(\beta_m - \theta)}{\cos\beta_m}\right) \tag{107}$$

The calculation of the total pressure drop is identical to that explained in Eqs. (58) - (61), except that, as mentioned cy_3^+ is now given by Eq. (98) rather than Eq. (56). In particular,the static pressure drop still follows from Eqs. (61 and (23), since only ideal flow through the bladed region is involved. Following calculation of $P_{t_o} - P_{t_{MIX.}}$, the efficiency and the loss parameter can be found as before (eqs. (63), (64)).

9.2 Comparison of the Theory with Partial Tip Loading to Data

In order to compare the modified theory of Sec. 9.1 to the same turbine data as before (Sec. 6.2), additional data regarding individual blade loading are needed to calculate the under-turning angle θ. This information is contained in the Zweifel coefficient ZW, which is also reported by Ref. 3 in each case, This is related to the blade lift as shown in Appendix B (Eq. B11). The angle θ then follows from Eq. 90, where the overall lift coefficient c_L is used as a representative value of the local c_L'.

The results for the same set of data as was used in Sec. 6.2 are summarized in Table 4, where the entries are the same as in Table 2, except for ZW and the last column, labelled K, which is the ratio of work done per unit mass by the underturned flow to that done by the blade-guided flow:

$$K = \frac{W^+}{W^-} \tag{108}$$

Once again, Case 1 can only be brought into agreement with the data if the load factor is reduced to about the design value (i.e., for zero exit swirl). Case No. 4, with very high reaction, is also substantially under-predicted, which may point ot an insufficient predicted underturning θ for these conditions. The rest of the cases are well predicted. Excluding Case 1, as before, the mean squared error is

$$\overline{\varepsilon^2} = 0.1162$$

and the mean error is

$$\bar{\varepsilon} = -0.1408$$

which imply a standard deviation

$$\sigma = 0.3105$$

These statistics are slightly better than those found for the zero tip loading theory (Sec. 6.2), and, although they compare favorably with those for the standard methods, they also still show some systematic under-prediction and moderate scatter. It is of interest that most of the error and scatter (other than that due to point 1) is caused by the single high-reaction data point (Case 4). If that entry were also removed, we would have $\overline{\varepsilon^2} = 0.0363$, $\bar{\varepsilon} = -0.0498$ and $\sigma = 0.184$.

Perhaps more effort should be devoted to an understanding of the leakage and underturning effects for high reaction rotors.

10. Summary and Conclusions

A theory has been developed to illuminate the effects of spanwise flow redistribution caused by the presence of a small rotor blade-tip gap. To this end, the blade-to-blade details are ignored by using an incomplete actuator disk formulation which collapses both startor and rotor to a plane, across which connecting conditions are imposed.

In the simplest version, the flow which leaks throught he tip gap is assumed to do zero work. The results indicate that the flow tends to go perferentially though the gap, and that the attendant flux reduction elsewhere is very nearly uniform in the spanwise direction. The axial length scale for this flow redistribution is the blade height, and not the gap size, as might have been expected. As a consequence, the unloading of the turbine blades is uniform, and the work defect cannot be localized in the near-gap region. On the other hand, the efficiency loss is due to mixing effects downstream of the gap. In this simple model, this mixing is that between the bulk flow and the underturned and somewhat axially faster stream going through the gap.

In order to shed some more light on the details of the gap flow, a modification was made to the theory in which the underturned stream was recognized as originating partly from gap flow, partly from entrained passage flow, both leaving the passage in the form of rolled-up tip vortex. The trajectory and other details of this vortex were calculated using a simple model involving the collision of the ideal pressure-driven leakage jet with the passage fluid. This model was calibrated against both, data and the theory of G.T. Cheng et al [12]. The modified actuator disk theory allows prediction of the fractional tip loading factor K, and introduces the effects of loading level on individual blades, which the simpler version ignores.

Both actuator disk models were then compared to a set of data involving 9 different turbines (10 operating conditions). With the

exception of one anomalous case, the calculated efficiency loss factors are reasonably close to the data, showing less deviation than the loss correlations of Ainley, Soderberg, Roelke, Kofskey and Lakhsminarayana.

These results suggest that upstream flow redistributions which have been largely ignored so far may be of importance in understanding the basic physics of tip leakage effects. It is recognized, however, that the complete smearing out of blade-to-blade variations may be too drastic an approximation, as the neglected scales are on the same order as the axial redistribution scale which is retained. Further work is recommended to explore this issue.

Acknowledgements

This work was supported by NASA Marshall SFC under Contract No. NAS8-35018 (Glenn E. Wilmer, Technical Monitor). The authors wish to acknowledge several useful discussions with Prof. F. Marble. This interaction was made possible through the support of the General Electric Turbo-machinery Research Fund.

Appendix A.

Disk versus Downstream Disturbances in Linearized Actuator Disk Theory

The linearized equation governing the streamline displacement $\tilde{z}$ in inverse coordinates is

$$\frac{1}{c_{xo}^2}\,\tilde{z}_{xx} + \tilde{z}_{\psi\psi} = -\frac{\omega_y(\Psi)}{(c_{ox}^3)} \tag{A1}$$

and $\omega_y \equiv 0$ for $x < o$. The boundary conditions (Eq. 29) are all homogeneous. The right-hand side of (A1) will be written for short as $R(x,\psi)$. To make it explicit that this must be replaced by zero for $x < o$, we introduce the unit step function $u(x)$ ($u=o$ for $x<o$, $u=1$ for $x>o$), and write

$$R(x,\psi) = r(\psi)\,u(x) \tag{A2}$$

where $r(\Psi) = -\omega_y(\Psi)/c_{xo}^3$. The function $R(x,\Psi)$ can be decomposed into its even and odd parts with respect to x:

$$R(x,\Psi) = \frac{1}{2}\,r(\Psi) + \left[u(x) - \frac{1}{2}\right] r(\Psi) \tag{A3}$$

The solution $\tilde{z}$ can then be broken into the part $\tilde{z}_H$, which satisfies the homogeneous equation, plus the forced solution, which will itself have even and odd components $\tilde{z}_E$ and $\tilde{z}_0$, corresponding to the decomposition (A3). Imposing the homogeneous boundary conditions (Eq. 29) on $\tilde{z}_H$ ensures that

$$\tilde{z}_H \equiv 0 \tag{A4}$$

The forced, even solution $\tilde{z}_E$ obeys (for all x)

$$\frac{1}{c_{xo}^2}\,(\tilde{z}_E)_{XX} + (\tilde{z}_E)_{\Psi\Psi} = \frac{1}{2}\,R(\Psi) \tag{A5}$$

and can therefore be taken as a function of Ψ alone, which leads to immediate integration

$$\tilde{z}_E = \frac{1}{2}\int^{\Psi}\left(\int^{\Psi_1} R(\Psi_2)\,d\Psi_2\right)d\Psi_1 + A\Psi + B \tag{A6}$$

with A and B chosen to satisfy $\tilde{z}_E(x,o) = \tilde{z}_E(x, H\,c_{xo}) = 0$.

The odd forced solution, $\tilde{z}_o$ must then be made to cancel $\tilde{z}_E(-\infty,\Psi)$.

$$\tilde{z}_0(-\infty,\Psi) = -\tilde{z}_E(\Psi) \tag{A7}$$

Therefore, at $x \rightarrow$, $\tilde{z}_0(-\infty,\Psi) = +\tilde{z}_E(\Psi)$, and superimposing,

$$\tilde{z}_0(-\infty,\Psi) = 2\,\tilde{z}_E(\Psi) \tag{A8}$$

On the other hand, since $\tilde{z}_0(x,\Psi)$ is odd in x, we have $\tilde{z}_0(0,\Psi) = 0$ so that

$$\tilde{z}_0(0,\Psi) = \tilde{z}_E(\Psi) \tag{A9}$$

Comparison of (A8) and (A9) proves that the displacement of each streamline is twice as large far downstream as it is at the disk.

Appendix B

Definition of Parameters Used in the Analysis

For convenient reference, we collect in this Appendix a number of performance parameters whose definitions vary sometimes from author to author. The form given here was used throughout our calculations.

B1. - Flow Coefficient

$$\phi = \frac{c_{x_o}}{U} \tag{B1}$$

B2. - Work Coefficient

$$\psi = \frac{\text{Power}}{\dot{m}\, U^2} \tag{B2}$$

For nominal conditions (no gap),

$$\psi = \phi\left(\tan \alpha_2 + \tan \beta_3\right) - 1 \tag{B3}$$

and if there is zero exit swirl $\left(\phi = 1/\tan \beta_3\right)$, then

$$\psi = \frac{\tan \alpha_2}{\tan \beta_3} \tag{B4}$$

B3. - Degree of Reaction

$$R = \frac{\text{Pressure drop in rotor}}{\text{Pressure drop in stage}} \tag{B5}$$

For zero gap (from Eqs. (23), (24),

$$R = \frac{\tan^2 \beta_3 - \left(\tan \alpha_2 - 1/\phi\right)^2}{2\dfrac{\tan \alpha_2}{\phi} - \left(\dfrac{1}{\phi^2} - \tan^2 \beta_3\right)} \tag{B6}$$

and if the exit swirl is zero $\left(\phi = 1/\tan \beta_3\right)$, then

$$R = 1 - \frac{\tan \alpha_2}{2 \tan \beta_3} \tag{B7}$$

B4. - Zweifel Coefficient

$$ZW = \frac{\text{Tangential force per Blade}}{\text{(Tangential Projected Area) x (Relative Exit Dynamic Head)}} \tag{B8}$$

For constant axial velocity,

$$ZW = 2 \left(\frac{s}{b}\right) \cos^2 \beta_3 \left(\tan \beta_2 - \tan \beta_3\right) \tag{B9}$$

where s = Azimutal blade spacing, and b = Axial depth of blading.

B5. - Blade Lift Coefficient

$$C_L = \frac{\text{Blade Lift}}{\text{(Blade Chord) x (Relative Inlet Dynamic Head)}} \tag{B10}$$

The ratio of ZW to C_L is just the ratio of the reference dynamic heads:

$$C_L = (ZW) \left(\frac{\cos \beta_2}{\cos \beta_3}\right)^2 \tag{B11}$$

References

1. J.S. Alford "Protecting Turbomachinery from Self-Excited Rotor Whirl". J. of Engineering for Power, Oct. 1965, pp. 338-344.

2. H.J. Thomas, "Instabile Eigenschwingungen von Turbinenlaufern, Angefacht durch die Spaltstromungen Stopfbuschenung Beschanfelungen." AEG-Sonderdruck, 1958. Also "Unstable Oscillations of Turbine Rotors due to Steam Leakage in the Clearance of the Sealing Glands and the Buckets", Bulletin Scientifique, A.J.M., Vol. 71, 1958, pp. 1039-1063.

3. W.F. Waterman "Turbine Loss Correlation and Analysis". Lecture presented at the Workshop on Tip Clearance Effects in Axial Turbomachines, Penn State Univ., April 14-18, 1986.

4. Rains D.A. "Tip Clearance Flows in Axial Flow Compressors and Pumps" CALTECH, Hydrodynamics and Mech. Engineering Labs., Report No. 5, 1954.

5. Vavra, M.H. Aerothermodynamics and Flow in Turbomachines, John Wiley, Inc. 1960.

6. Lakshminarayana, B. "Methods of Predicting the Tip Clearance Effects in Axial Flow Turbomachinery". ASME Journal of Basic Engineering, Vol. 104, pp. 467-481, 1970.

7. Lakshminarayana, B. and Horlock, J.H. "Tip Clearance Flow and Losses for an Isolated Compressor Blade". ARC R&M 3316, 1962.

8. Lewis, R.I. and Yeung, E.H.C. "Vortex Shedding Mechanisms in Relation to Tip Clearance Flows and Losses in Axial Fans", ARC R&M 3829, 1977.

9. Adamczyk, J.J., Celestina, M.A. Beach, T.A. and Barnett, M. "Simulation of Three-Dimensional Viscous Flow Within a Multi-Stage Turbine' ASME Paper 89-GT-152, Toronto, Canada, 1989.

10. A.J. Crook "Numerical Investigation of Endwall/Casing Treatment Flow Phenomena". M.S. Thesis, M.I.T., Dept of Aeronautics/Astronautics, Aug. 1989.

11. Horlock, J.H., Actuation Disc Theory, McGraw-Hill, 1978.

12. Robert P. Gauthier, "An Investigation of Flow Field Perturbation Caused by Constant Blade-Tip Clearance in a Turbine", M.S. Thesis, M.I.T., Dept of Aeronautics/Astronautics, 1990.

13. G.T. Chen, E.M. Greitzer, C.S. Tan and F.E. Marble, "Similarity Analysis if Compressor Tip Clearance Flow Structure". To be presented at the 1990 ASME Gas Turbine Conference.

14. G.K. Batchelor, An Introduction to Fluid Dynamics, Cambridge U. Press, 1967. Section 7.3.

TABLE 1
MEAN SQUARED ERROR AND MEAN ERROR MAGNITUDE FOR VARIOUS TIP LOSS CORRELATIONS (FROM REF. 3)

	$\frac{1}{N}\sum\left(\frac{\Delta\eta}{\Delta\tau/h}\Big\vert_{PRED} - \frac{\Delta\eta}{\Delta\tau/h}\Big\vert_{EXP}\right)^2$	$\frac{1}{N}\sum\left(\frac{\Delta\eta}{\Delta\tau/h}\Big\vert_{PRED} - \frac{\Delta\eta}{\Delta\tau/h}\Big\vert_{EXP}\right)$
Kofskey	0.227	-0.093
Ainley	1.186	-0.074
Soderberg	0.638	0.500
Roelke	0.192	0.235

CASE #	AUTHOR	ϕ	Ψ_o	R	δ/H	$(\beta)_{DATA}$	$(\beta)_{CALC.}$	$(w)_{CALC.}$	$\left(\frac{c_y}{c_{x_o}}\right)_{CALC.}$
1	KOFSKEY	0.79	7.0	0.02	0.05	1.02	3.032	1.020	-3.199
2A	MARSHALL -ROGO	0.50	1.48	0.32	0.035	1.51	1.156	1.541	-0.105
2B	MARSHALL -ROGO	0.44	1.25	0.35	0.035	1.23	1.068	1.663	+0.076
3	SZANCA-BEHNING-SCHUM	0.57	1.46	0.47	0.033	1.90	1.449	1.987	-0.336
4	HOLESKI-FUTRAL	0.26	0.69	0.69	0.031	2.53	1.883	5.644	+0.042
5	EWEN-HUBER -MITCHELL	0.25	1.05	0.45	0.02	1.50	1.294	2.328	0.136
6	LART	0.51	1.41	0.51	0.02	1.80	1.645	2.304	-0.416
7	YAMAMOTO	0.42	1.52	0.47	0.03	1.63	1.652	2.166	-0.528
8	PATEL	0.28	1.15	0.61	0.01	1.81	2.438	4.155	-0.648
9	HAAS-KOFSKEY	0.35	1.37	0.47	0.03	1.80	1.564	2.251	-0.408
1 (MODIFIED)	KOFSKEY (Assuming Ψ_o=2)	0.79	2.0	0.02	0.05	1.02	0.973	1.019	-0.025
8 (MODIFIED)	PATEL (Assuming Ψ_o=0.83)	0.28	0.83	0.61	0.01	1.81	1.823	4.234	-0.052

TABLE 2 Efficiency loss and work defect calculated from theory (assuming zero work done by gap fluid), compared to data. The last two lines are computed with modified work coefficients chosen for near-axial exit flow

Table 3 Axial and radial velocities at x=0 for two grid sizes

	Grid 16X32	Grid 24X48
ϕ	$(C_x)_{x=0}$	$(C_x)_{x=0}$
.9750	1.36396	1.36279
.9250	.97904	.97962
.9000	.98285	.98326

ϕ	$(C_z)_{x=0}$	$(C_z)_{x=0}$
.9750	.13404	.13677
.9250	.14692	.15054
.9000	.09922	.09976

CASE #	AUTHOR	ZW	ϕ	Ψ_o	R	δ/H	$(\beta)_{DATA}$	$(\beta)_{CALC.}$	$(w)_{CALC.}$	$K_{CAL.}$
1	KOFSKEY	55	0.79	7.0	0.02	0.05	1.02	2.902	4.096	1.025
2A	MARSHALL -ROGO	1.02	0.50	1.48	0.32	0.035	1.51	1.443	2.563	0.346
2B	MARSHALL -ROGO	1.09	0.44	1.25	0.35	0.035	1.23	1.418	2.757	0.290
3	SZANCA-BEHNING-SCHUM	1.59	0.57	1.46	0.47	0.033	1.90	1.681	3.066	0.369
4	HOLESKI-FUTRAL	0.35	0.26	0.69	0.69	0.031	2.53	1.661	4.880	0.365
5	EWEN-HUBER -MITCHELL	0.70	0.25	1.05	0.45	0.02	1.50	1.458	3.914	0.411
6	LART	0.92	0.51	1.41	0.51	0.02	1.80	1.924	3.500	0.375
7	YAMAMOTO	0.79	0.42	1.52	0.47	0.03	1.63	1.803	3.558	0.452
8	PATEL	0.70	0.28	1.15	0.61	0.01	1.81	1.415	4.813	0.683
9	HAAS-KOFSKEY	0.80	0.35	1.37	0.47	0.03	1.80	1.640	4.714	0.468
1 (MODIFIED)	KOFSKEY (Assuming Ψ_o=2)	0.55	0.79	2.0	0.02	0.05	1.02	0.926	1.614	0.473

TABLE 4 Efficiency loss and work defect calculated from theory (including allowance for partial tip loading), compared to data. The last line is computed with modified work coefficient chosen for near-axial exit flow

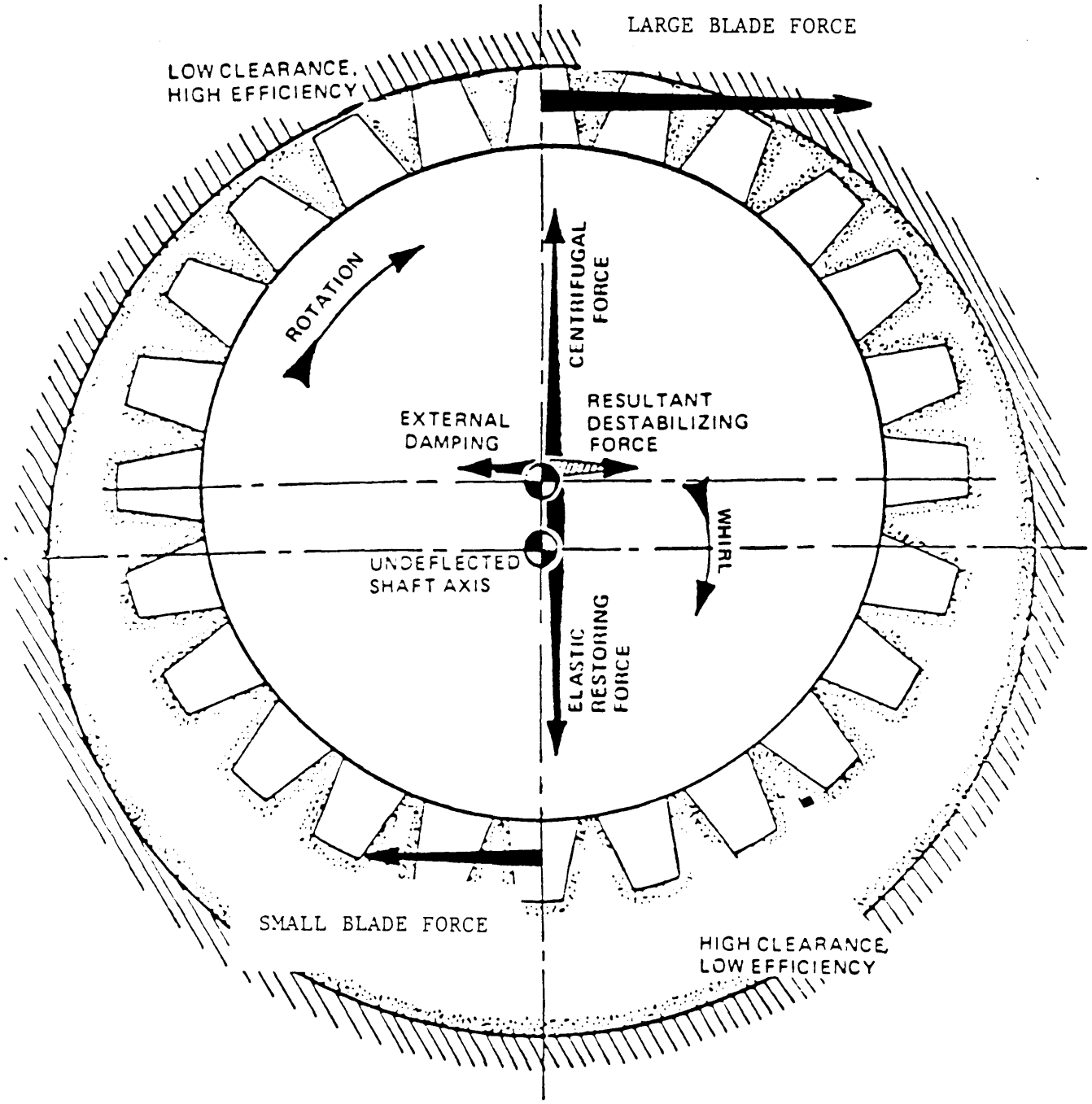

Fig. 1: Contribution to whirl from turbine tip clearance effects

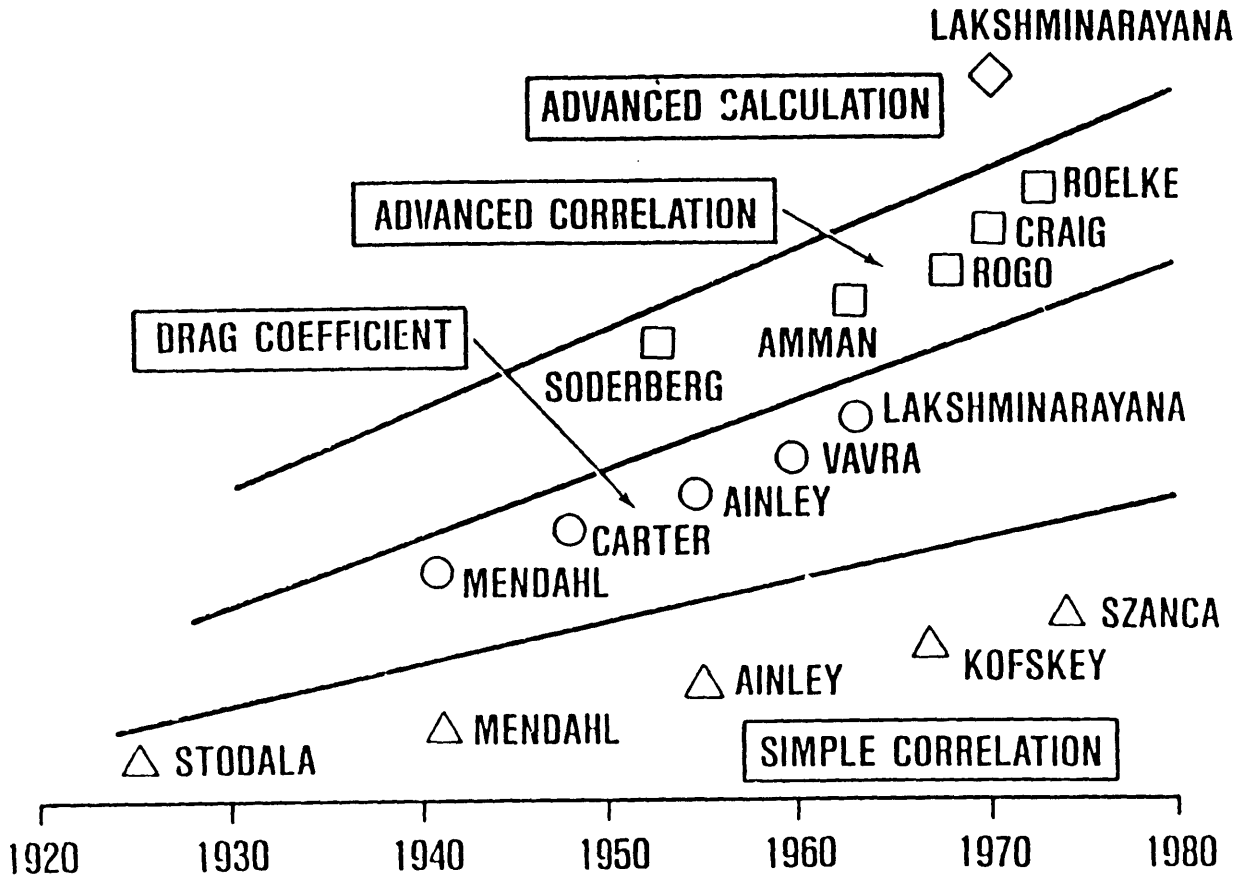

Fig. 2: Various levels of blade-tip loss theory (from Waterman, Ref. 3)

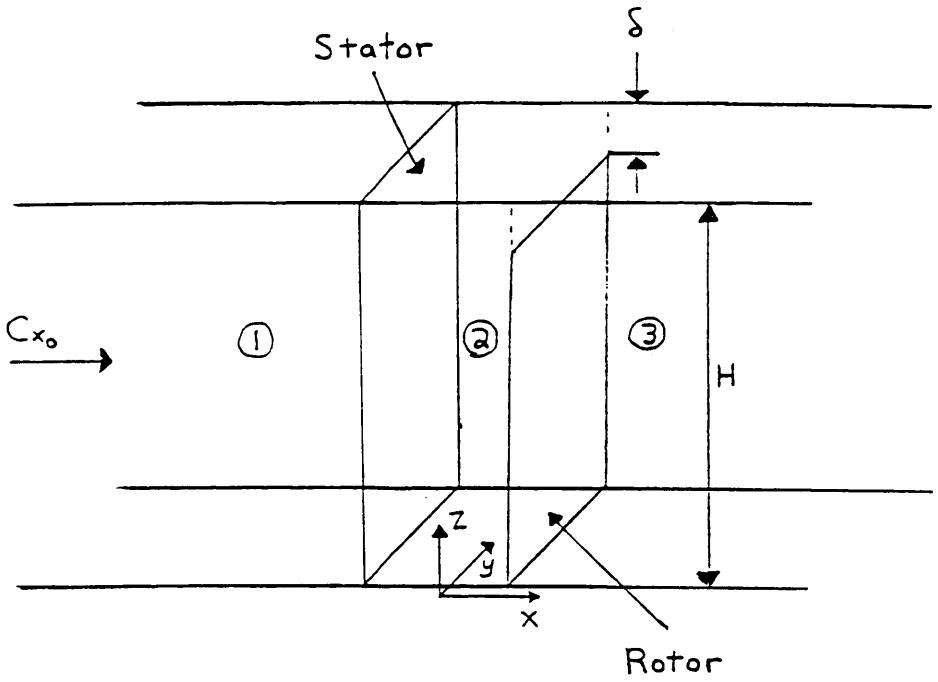

Fig. 3: Channel flow with constant blade-tip clearance

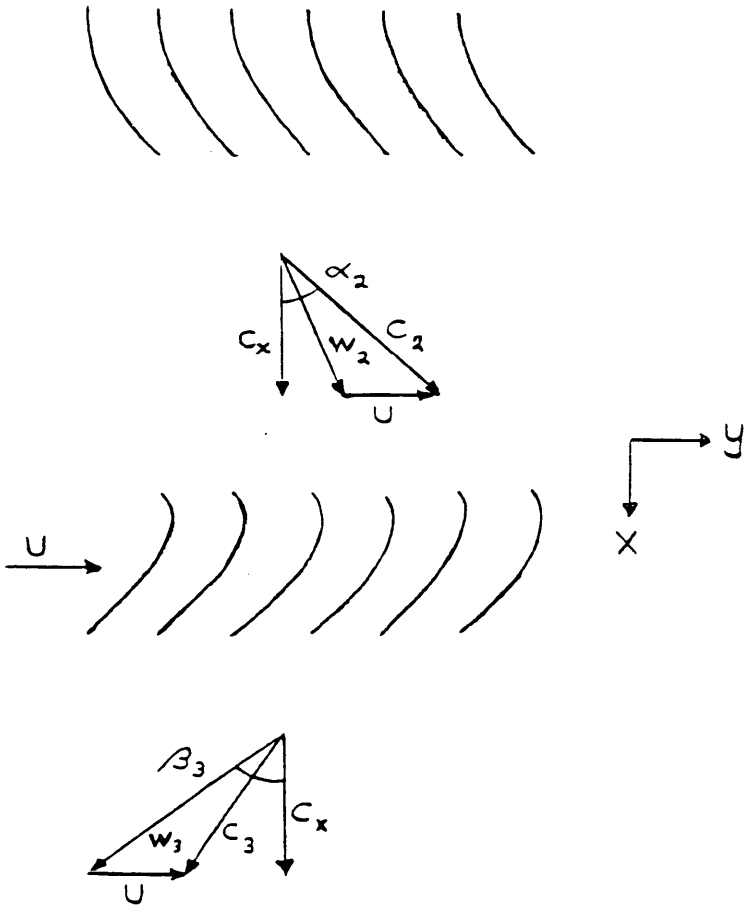

Fig. 4: Velocity triangles

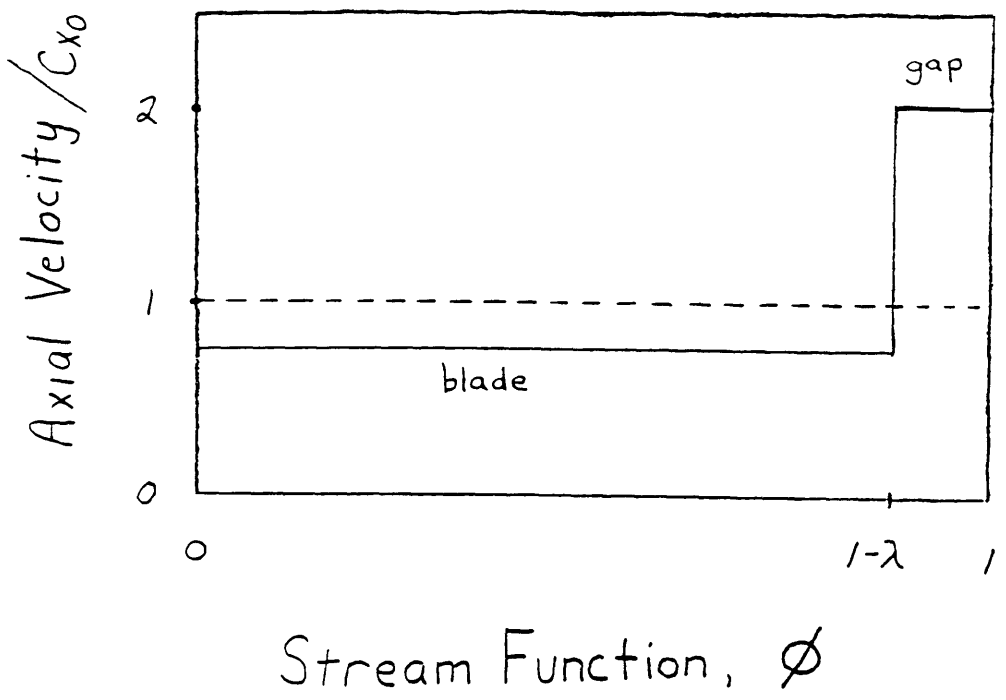

Fig. 5: Axial velocity distribution at disk

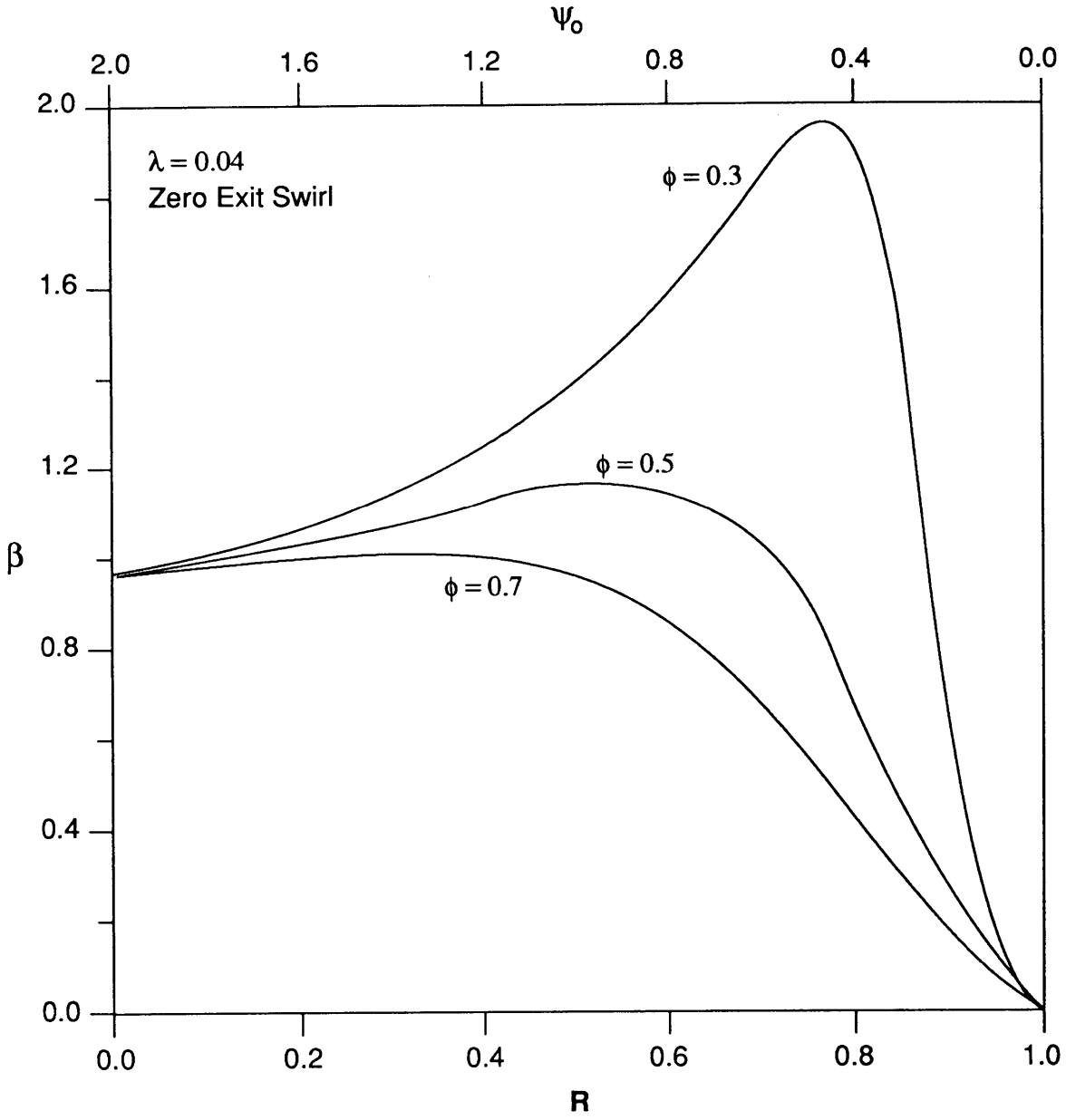

Fig. 6: Loss parameter variation with loading or degree of reaction for zero exit swirl (leakage fixed)

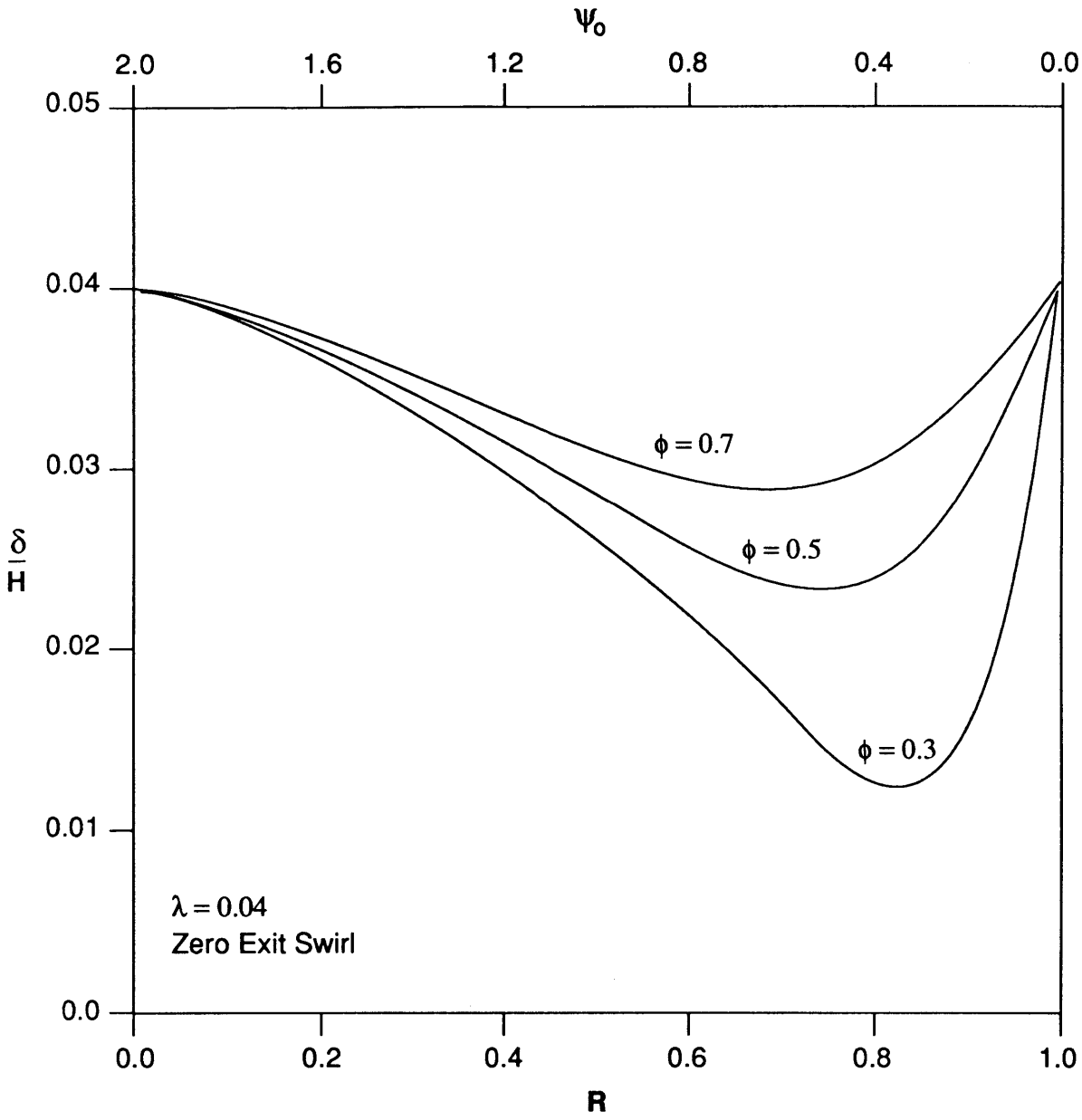

Fig. 7: Gap variation for conditions of Fig. 6

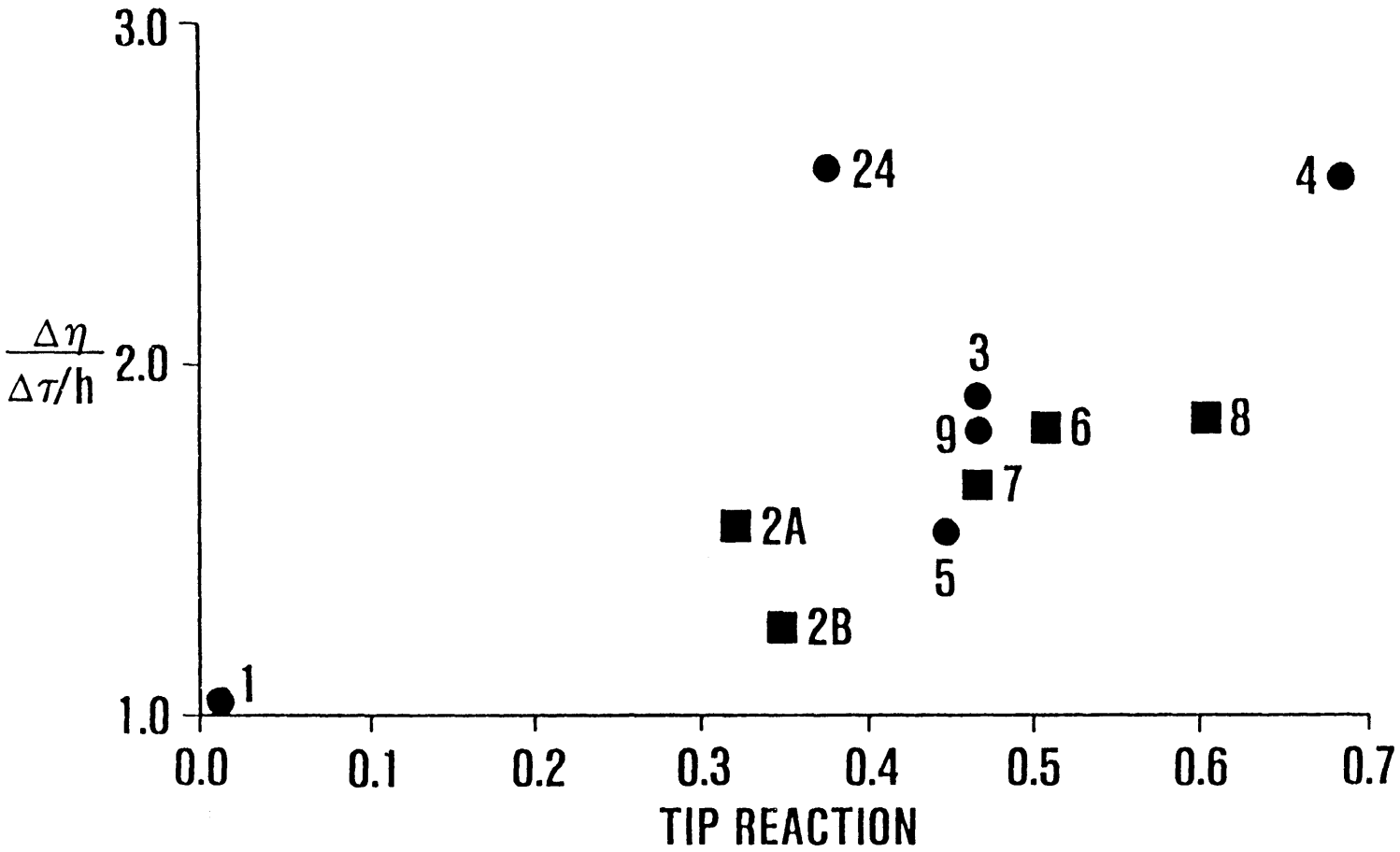

Fig. 8: Data collected by Ref. 3 indicate a trend of losses to increase with degree of reaction

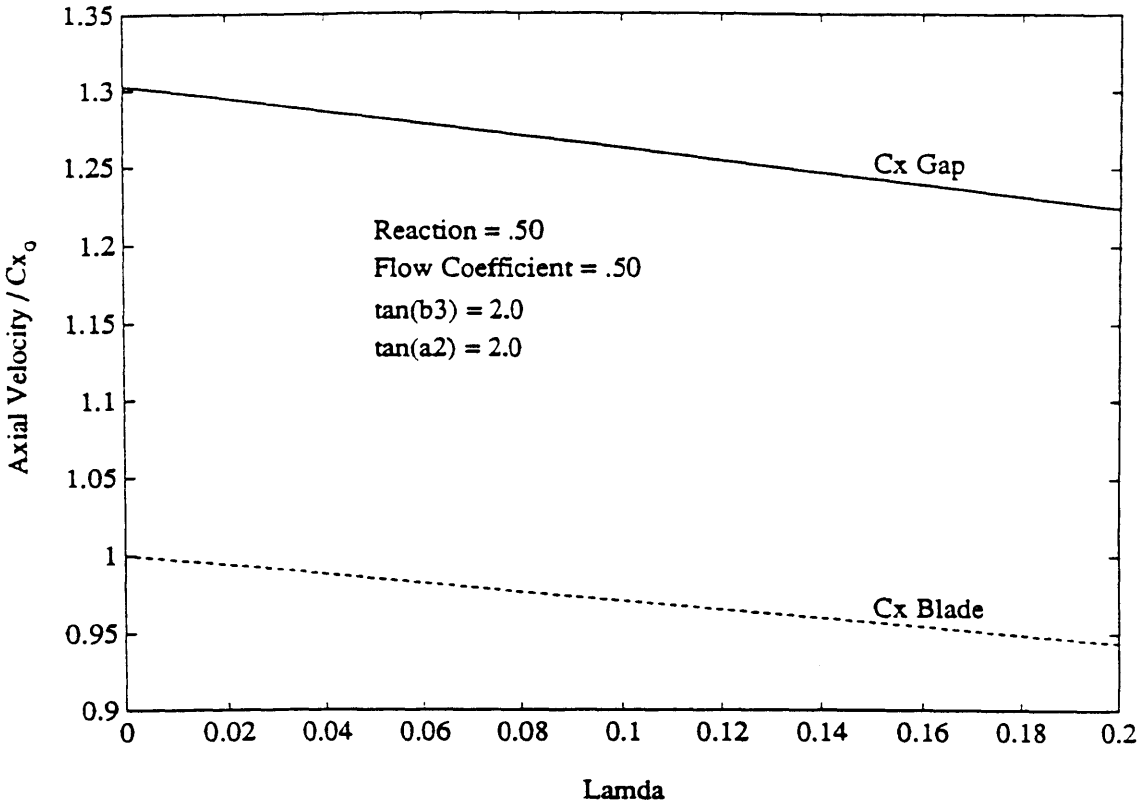

Fig. 9: Variation of axial velocity levels at disk with leakage

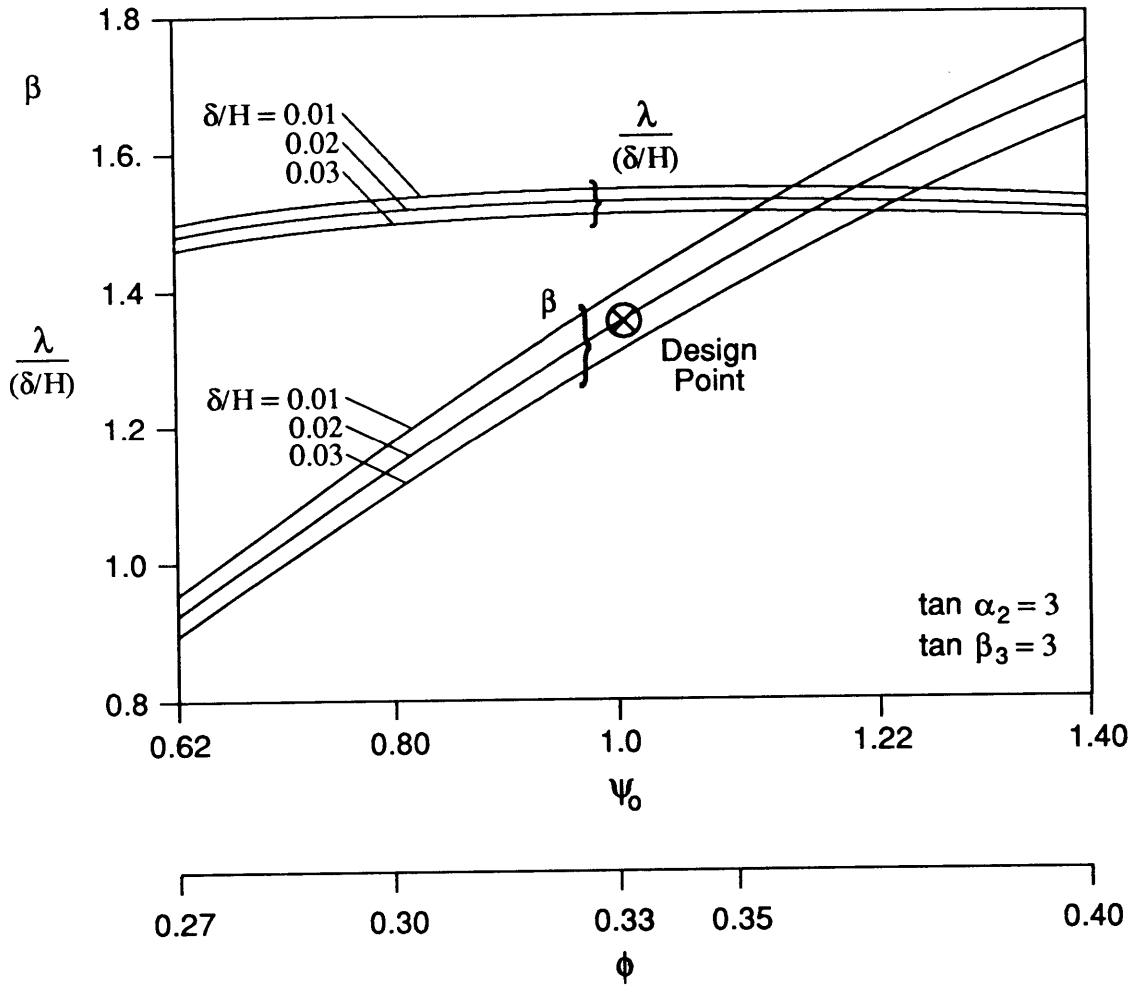

Fig. 10: Variation of losses and leakage rate with flow coefficient for a fixed geometry

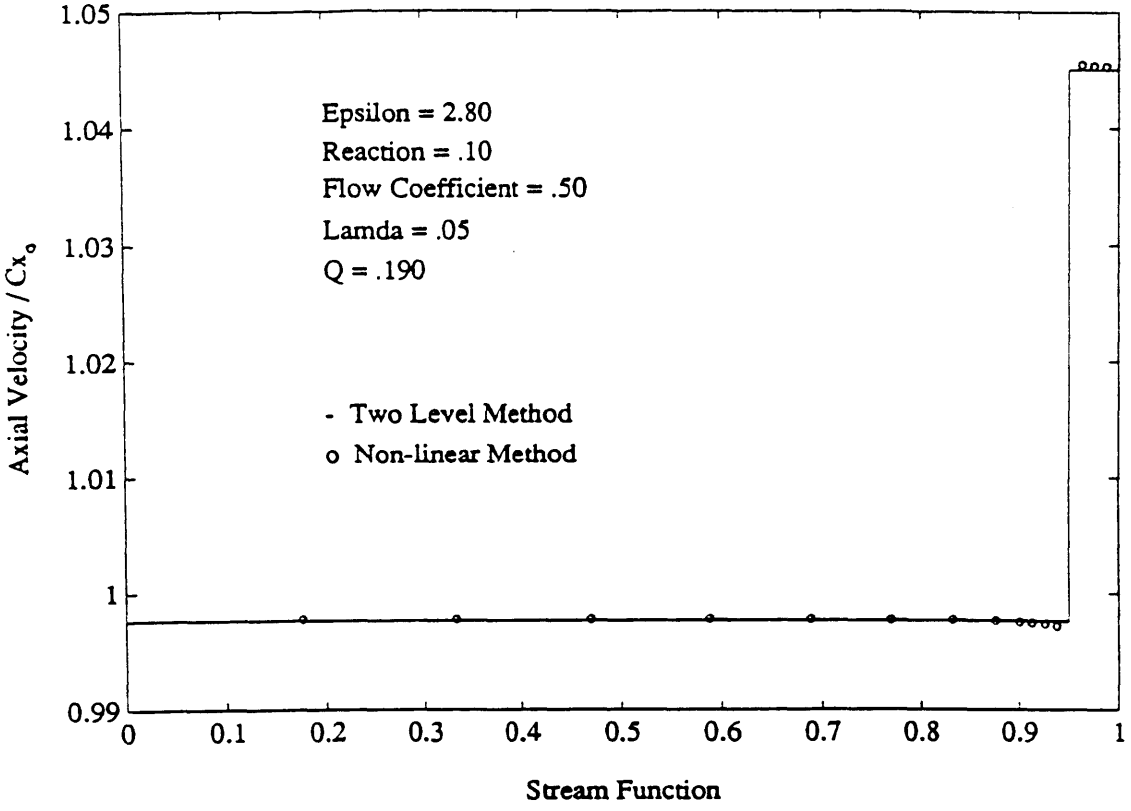

Fig. 11: Numerical vs. analytical axial velocity profiles at disk

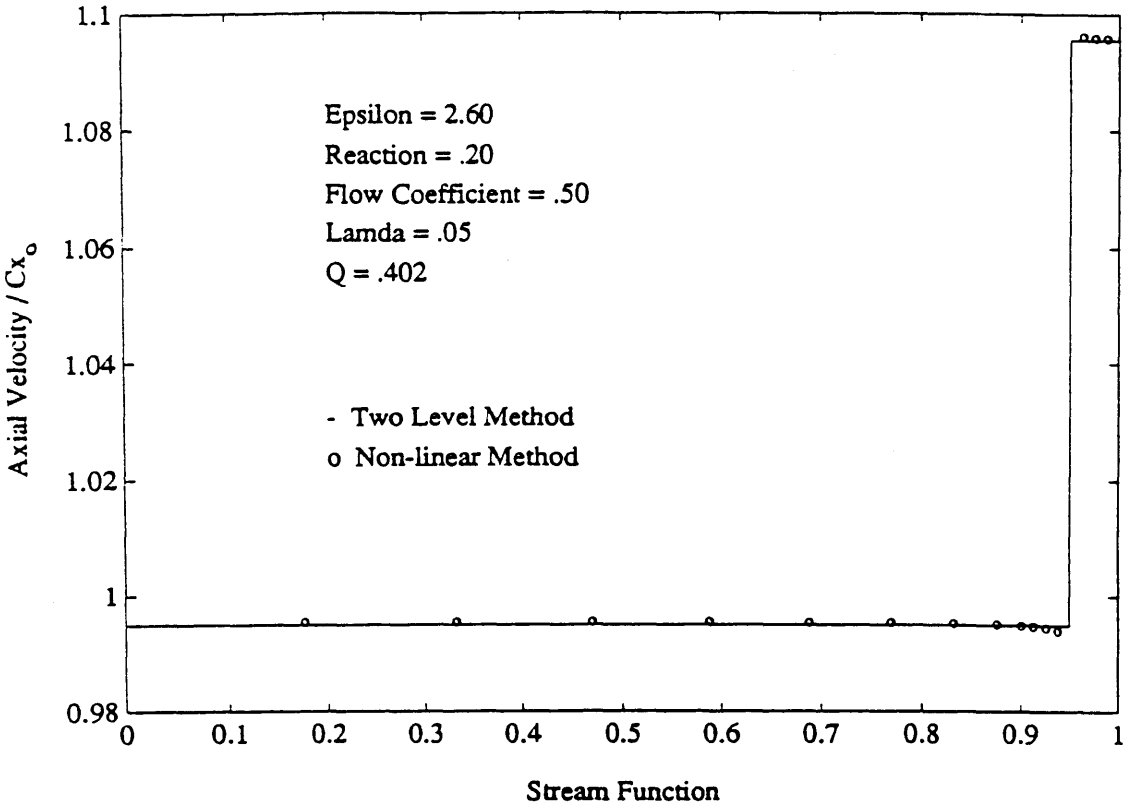

Fig. 12: Numerical vs. analytical axial velocity profiles at disk

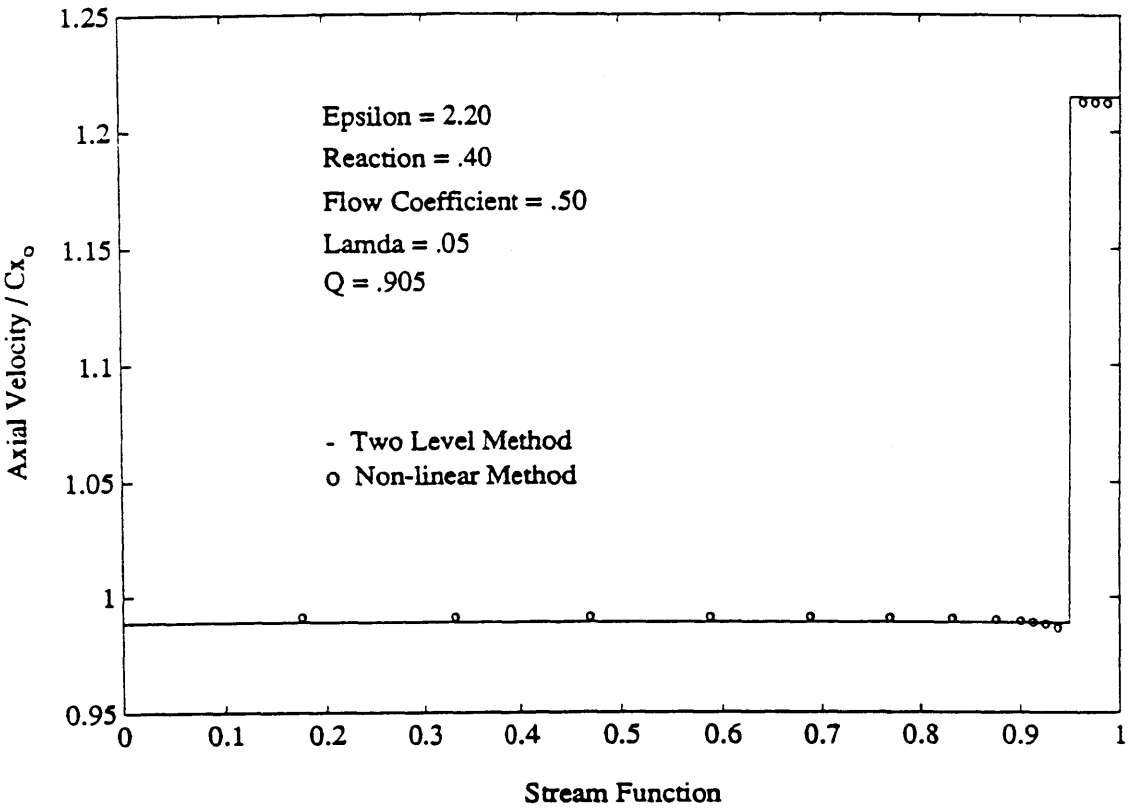

Fig. 13: Numerical vs. analytical axial velocity profiles at disk

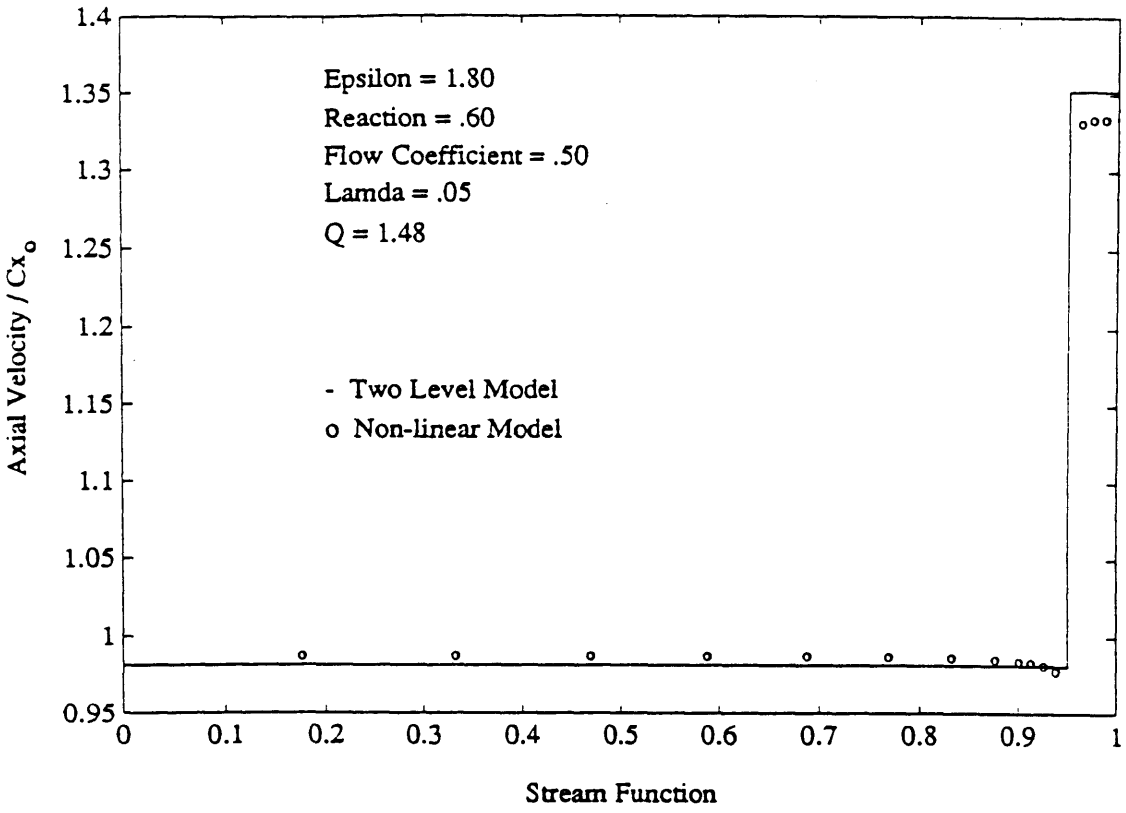

Fig. 14: Numerical vs. analytical axial velocity profiles at disk

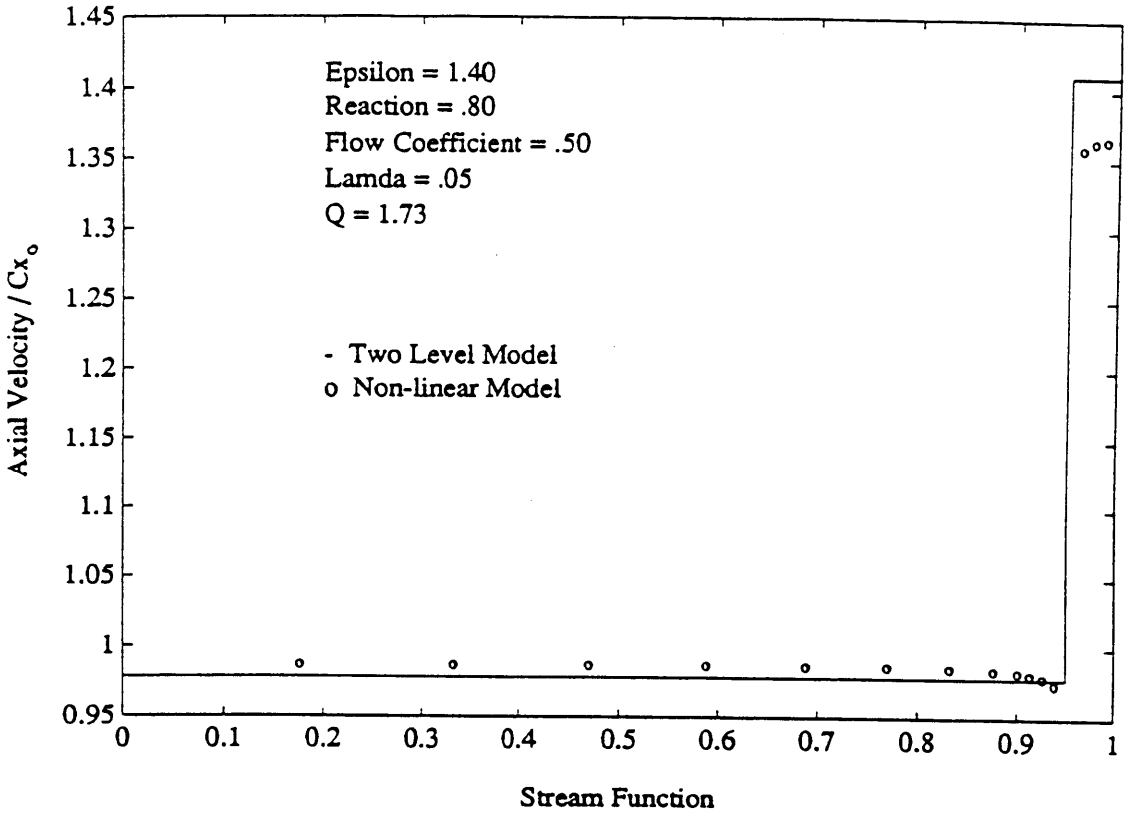

Fig. 15: Numerical vs. analytical axial velocity profiles at disk

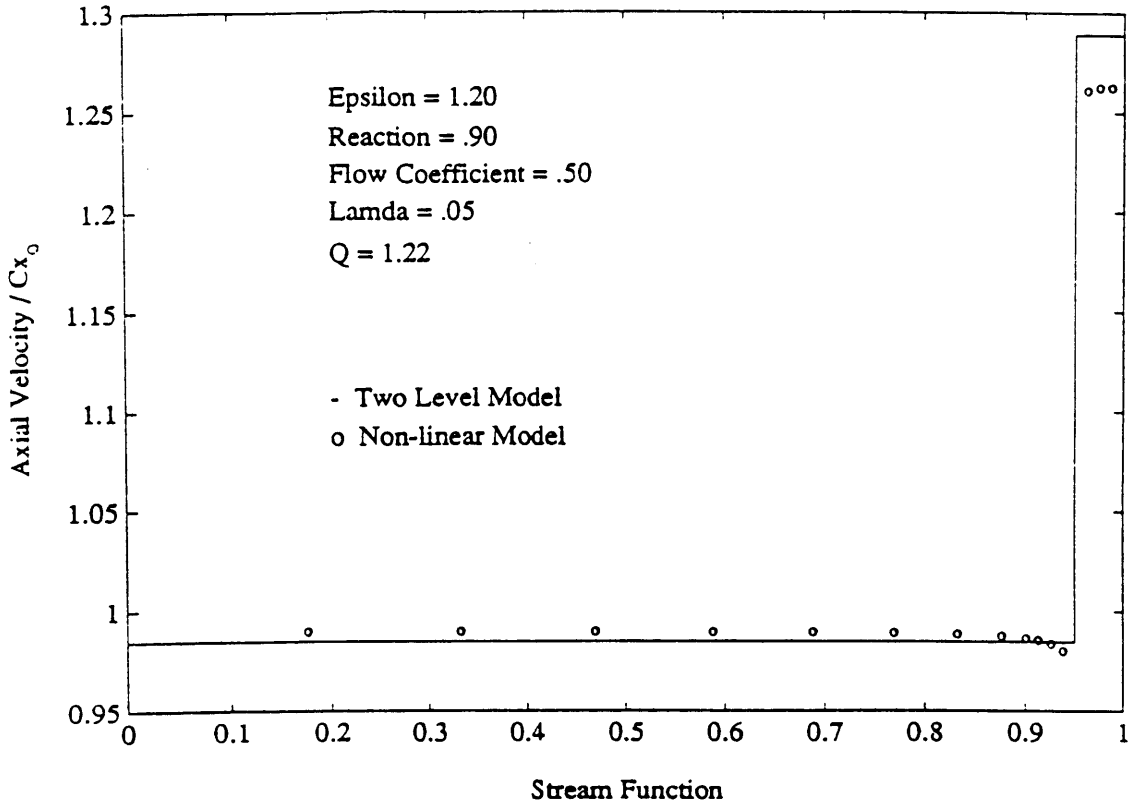

Fig. 16: Numerical vs. analytical axial velocity profiles at disk

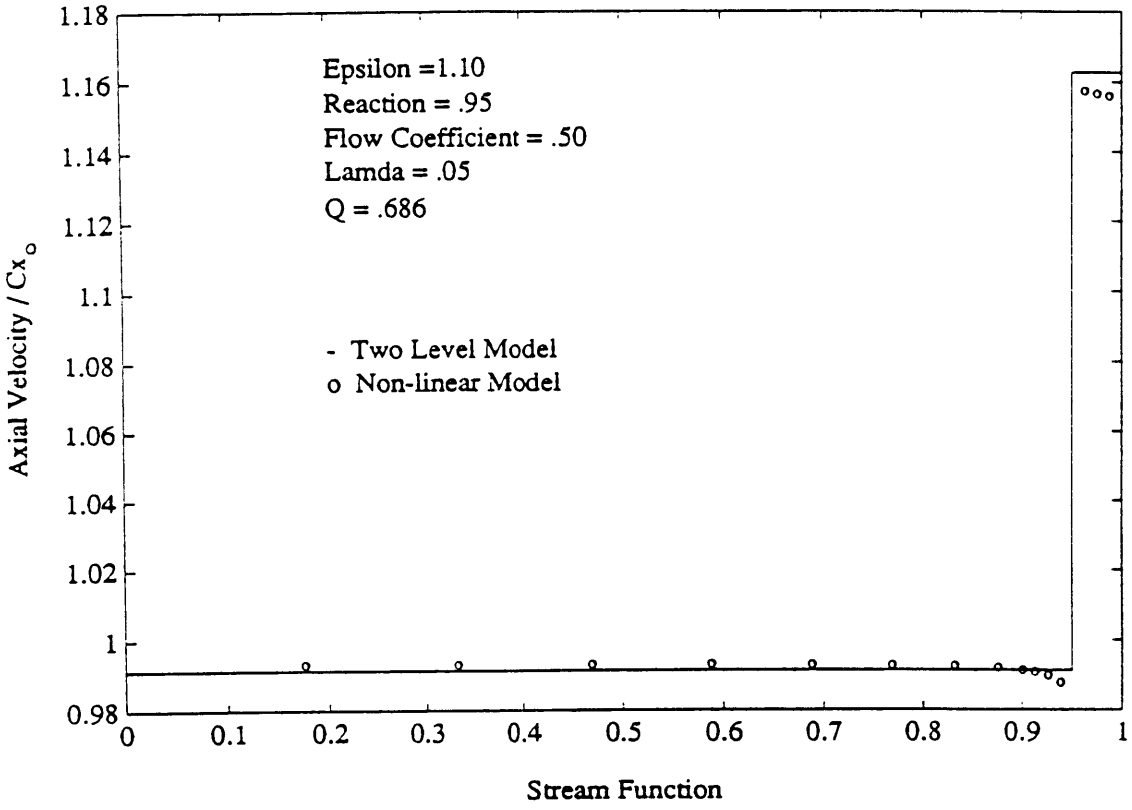

Fig. 17: Numerical vs. analytical axial velocity profiles at disk

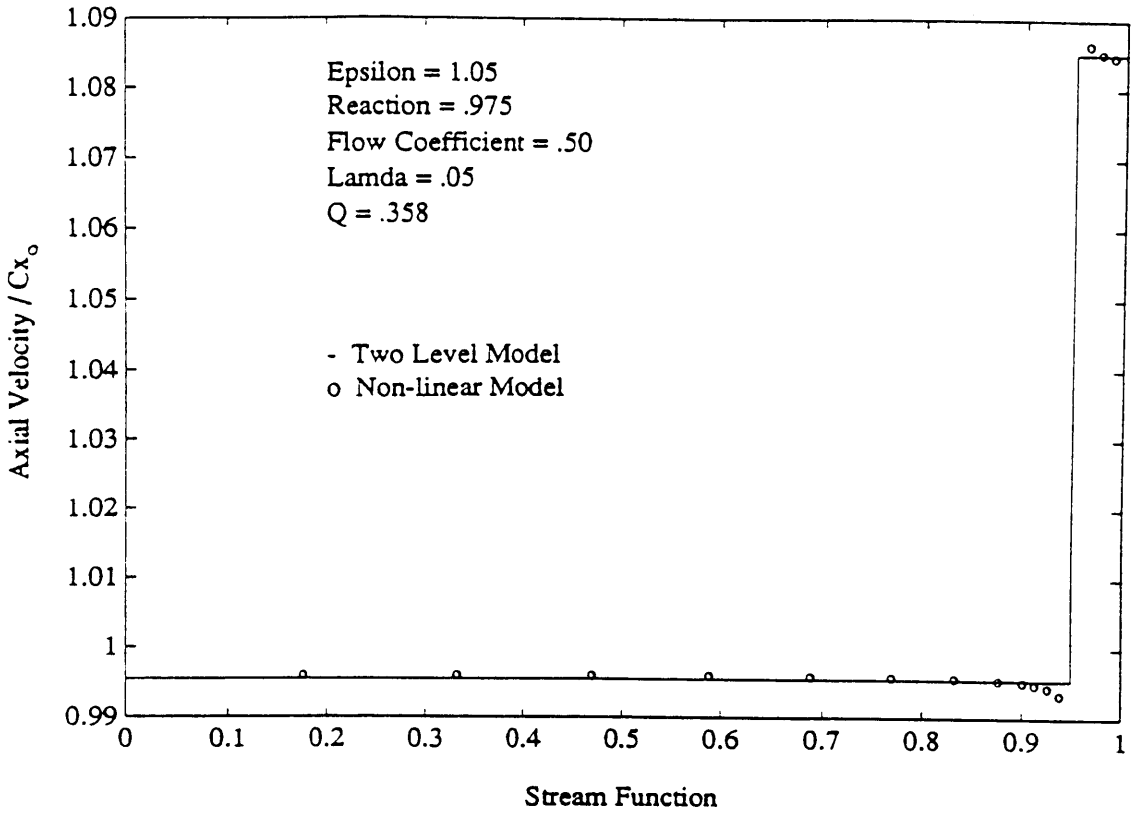

Fig. 18: Numerical vs. analytical axial velocity profiles at disk

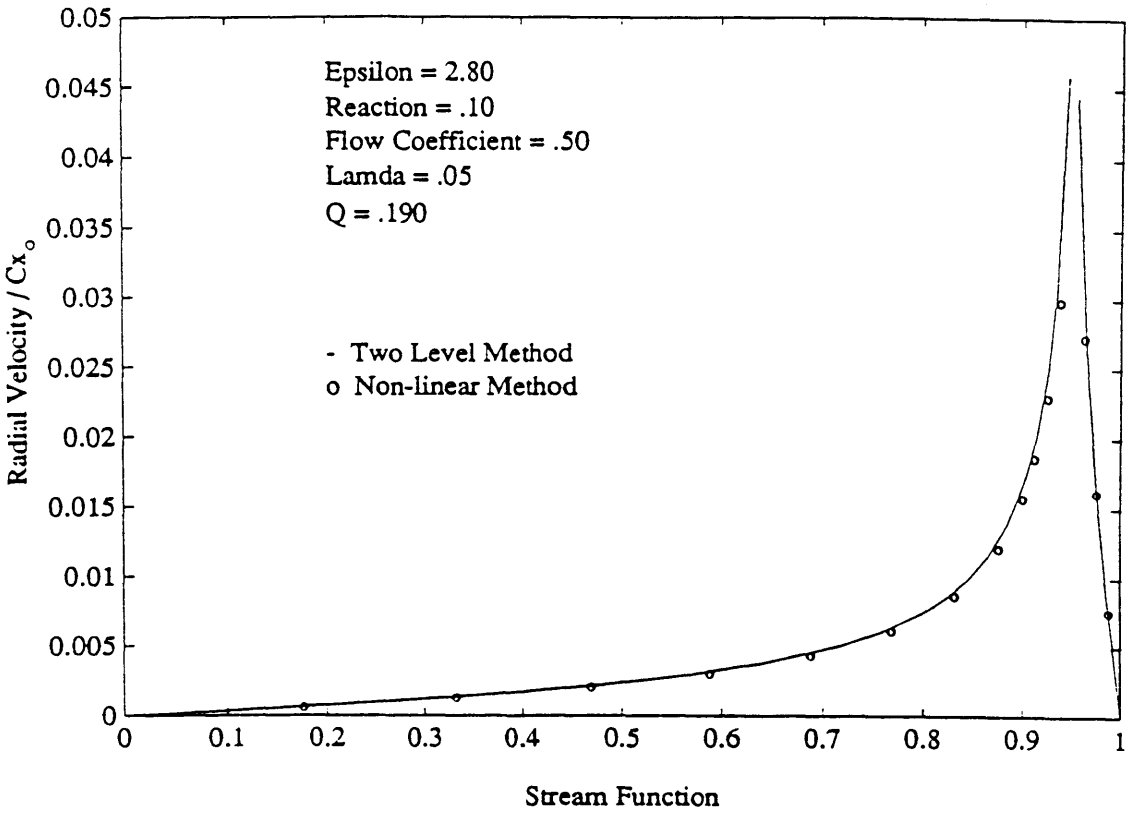

Fig. 19: Numerical vs. analytical spanwise velocity profiles at disk

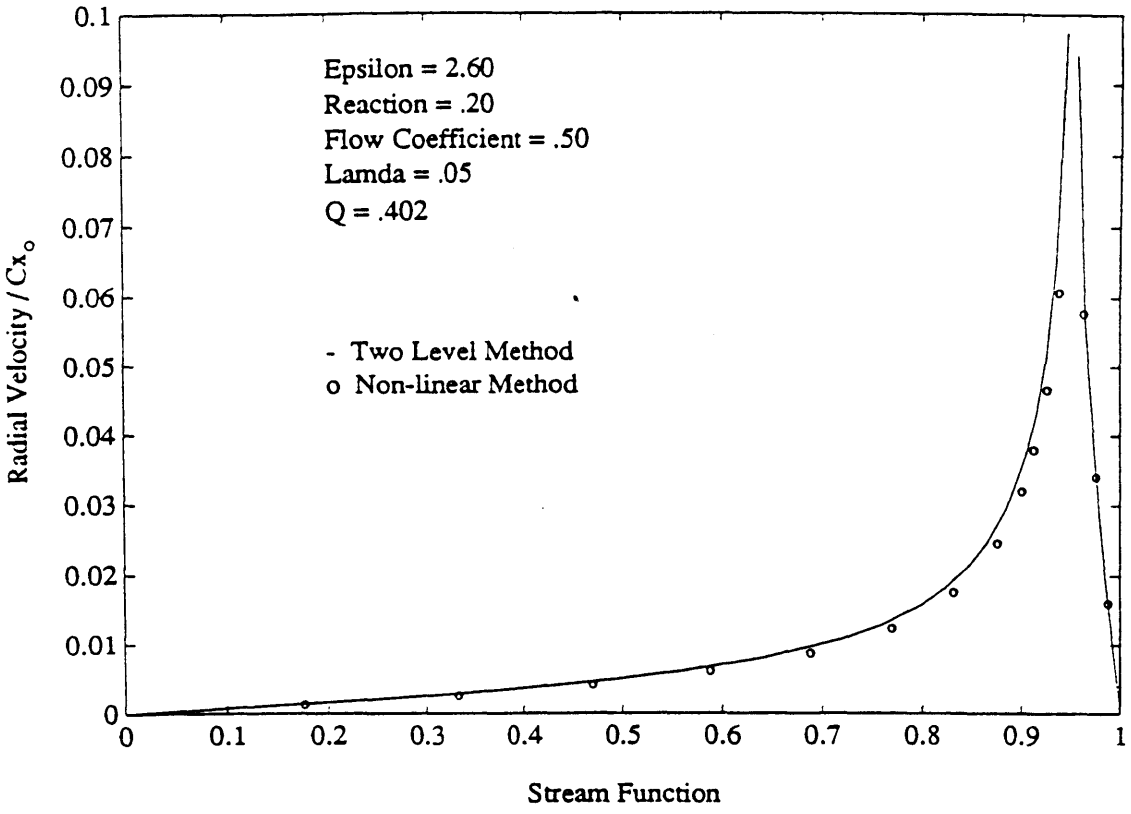

Fig. 20: Numerical vs. analytical spanwise velocity profiles at disk

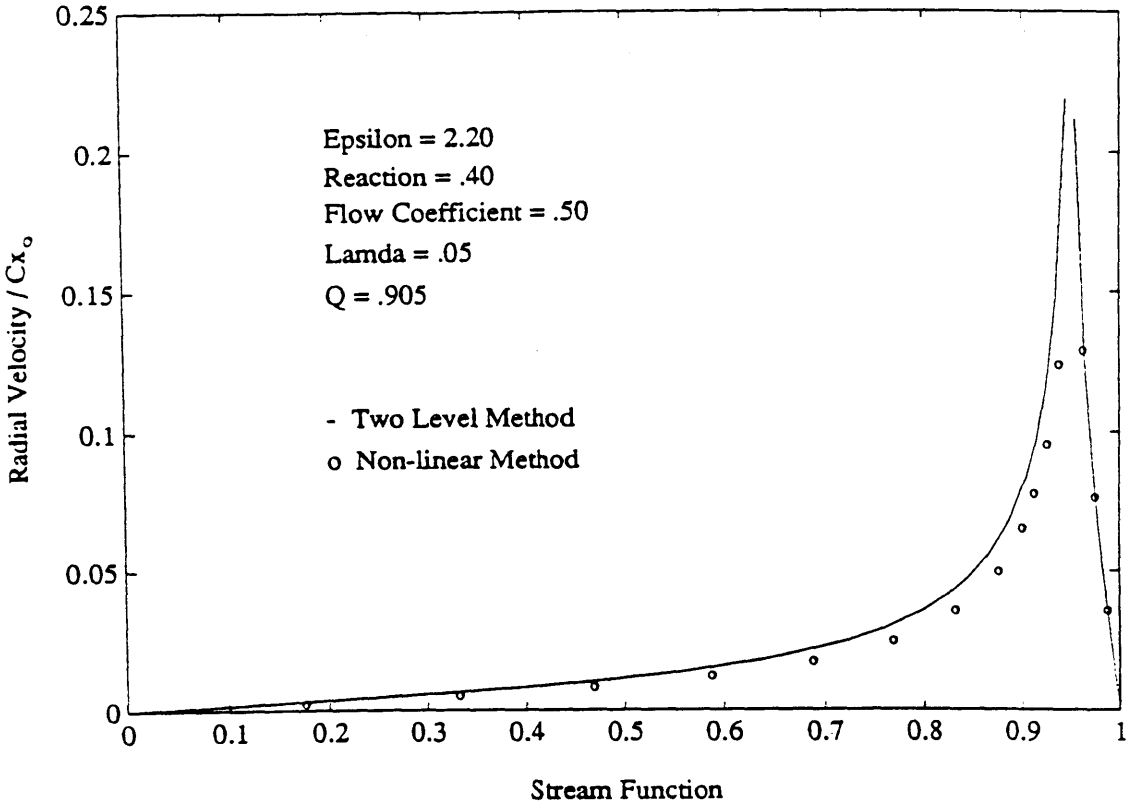

Fig. 21: Numerical vs. analytical spanwise velocity profiles at disk

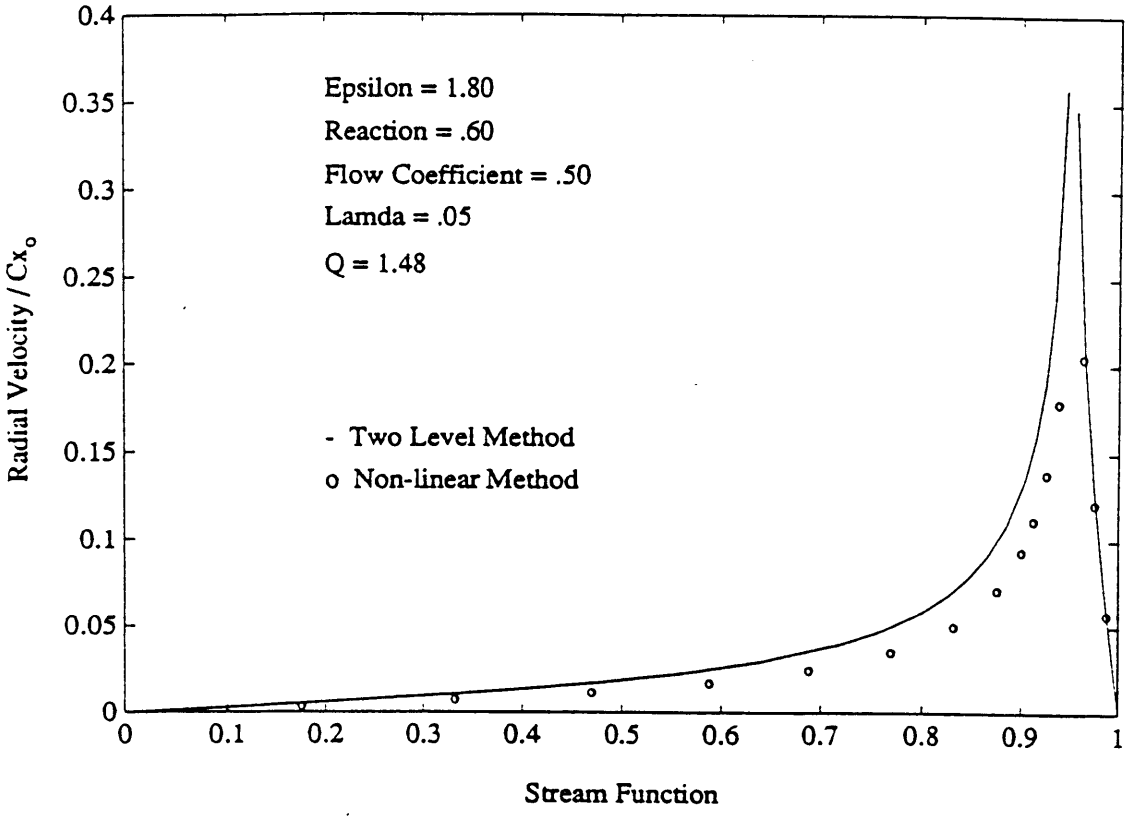

Fig. 22: Numerical vs. analytical spanwise velocity profiles at disk

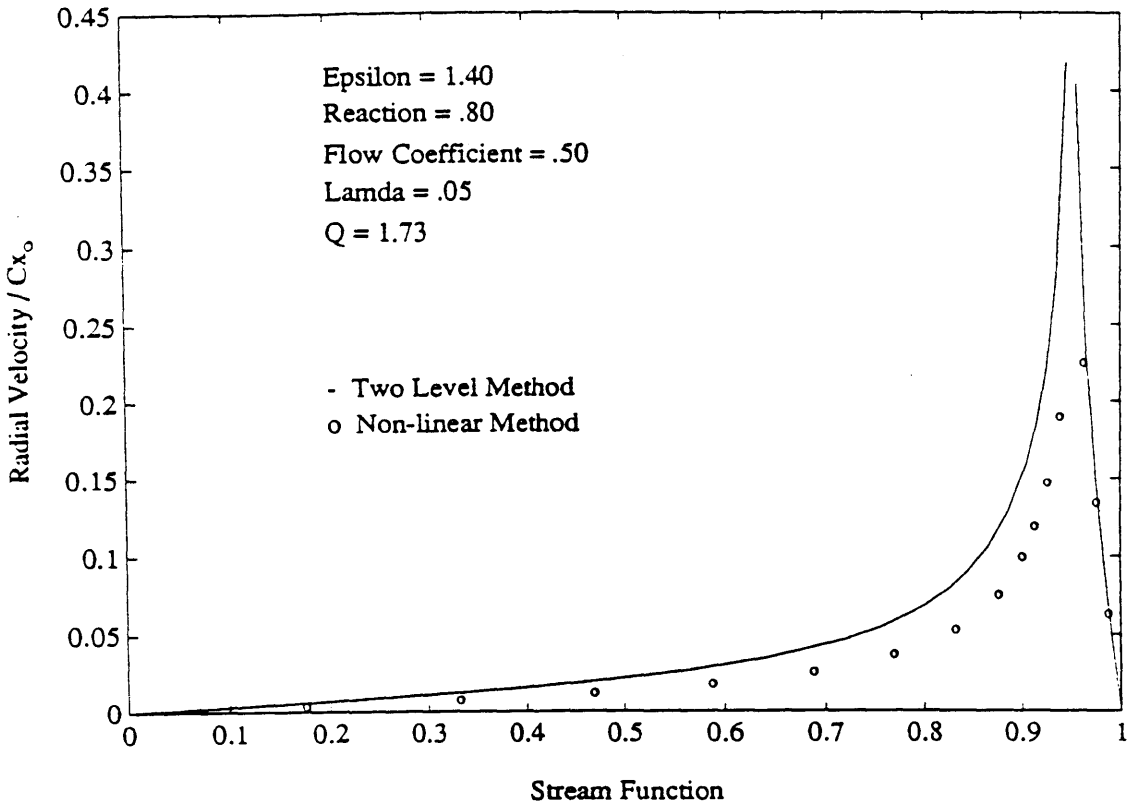

Fig. 23: Numerical vs. analytical spanwise velocity profiles at disk

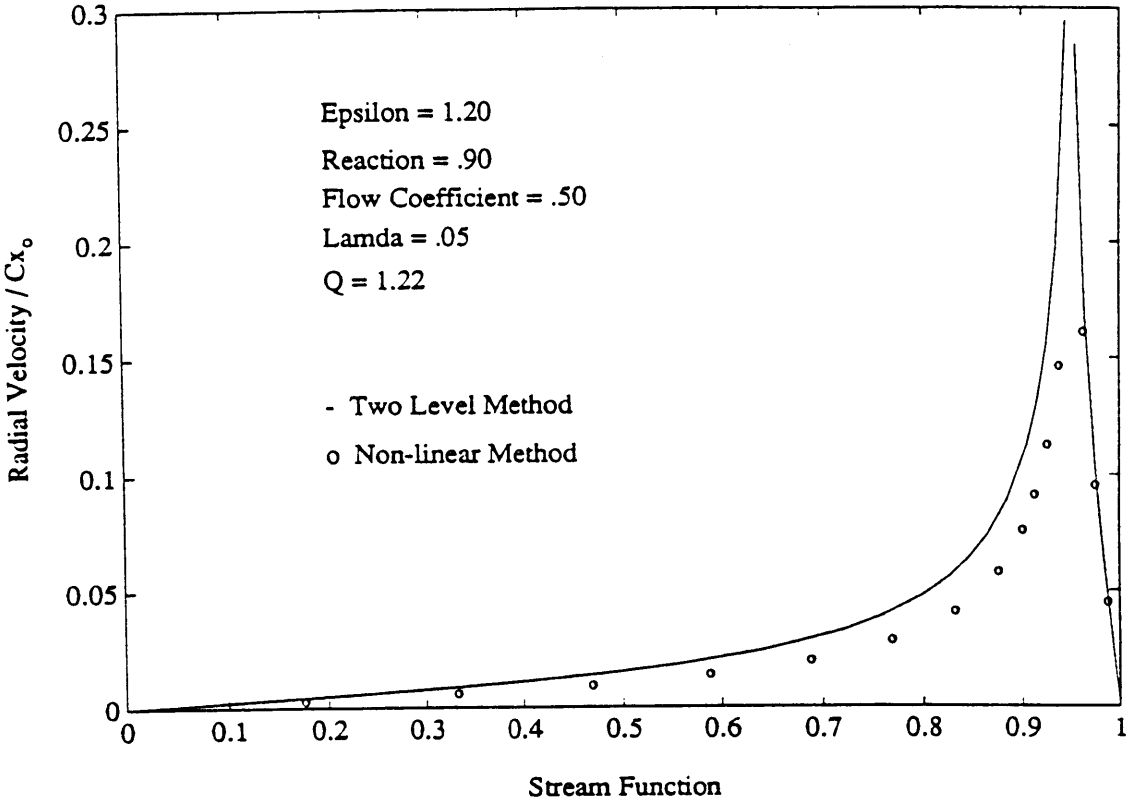

Fig. 24: Numerical vs. analytical spanwise velocity profiles at disk

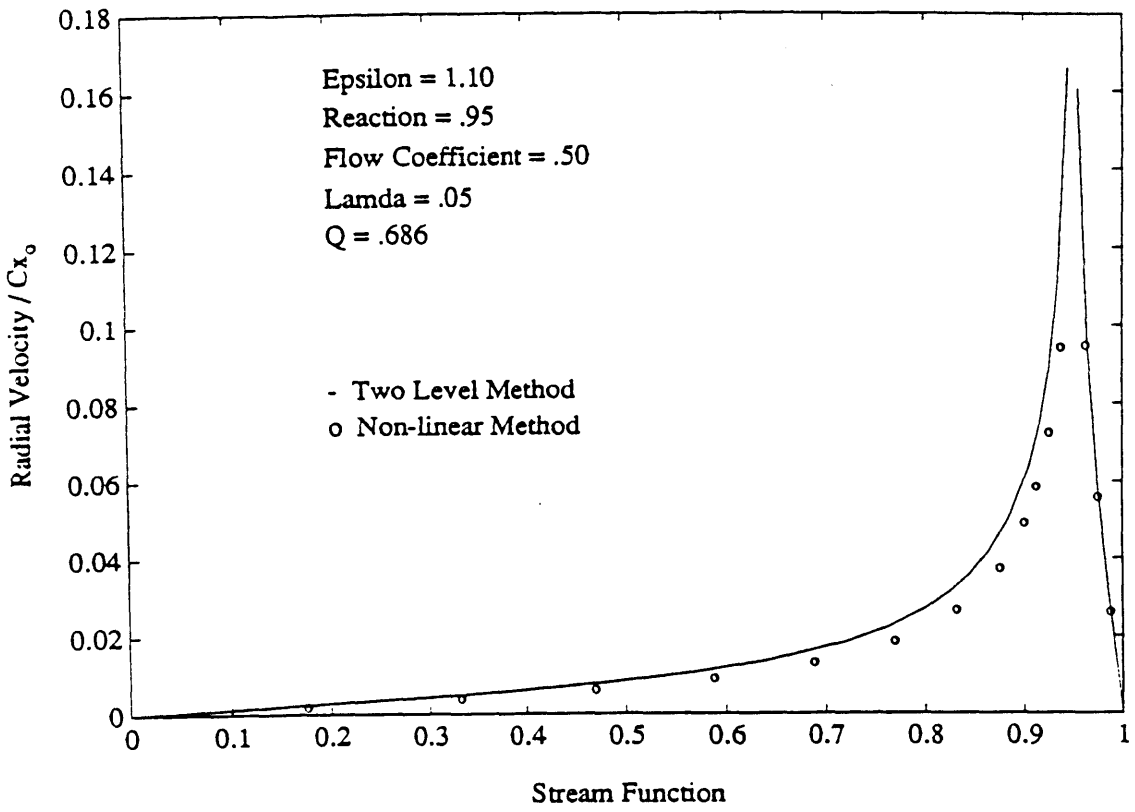

Fig. 25: Numerical vs. analytical spanwise velocity profiles at disk

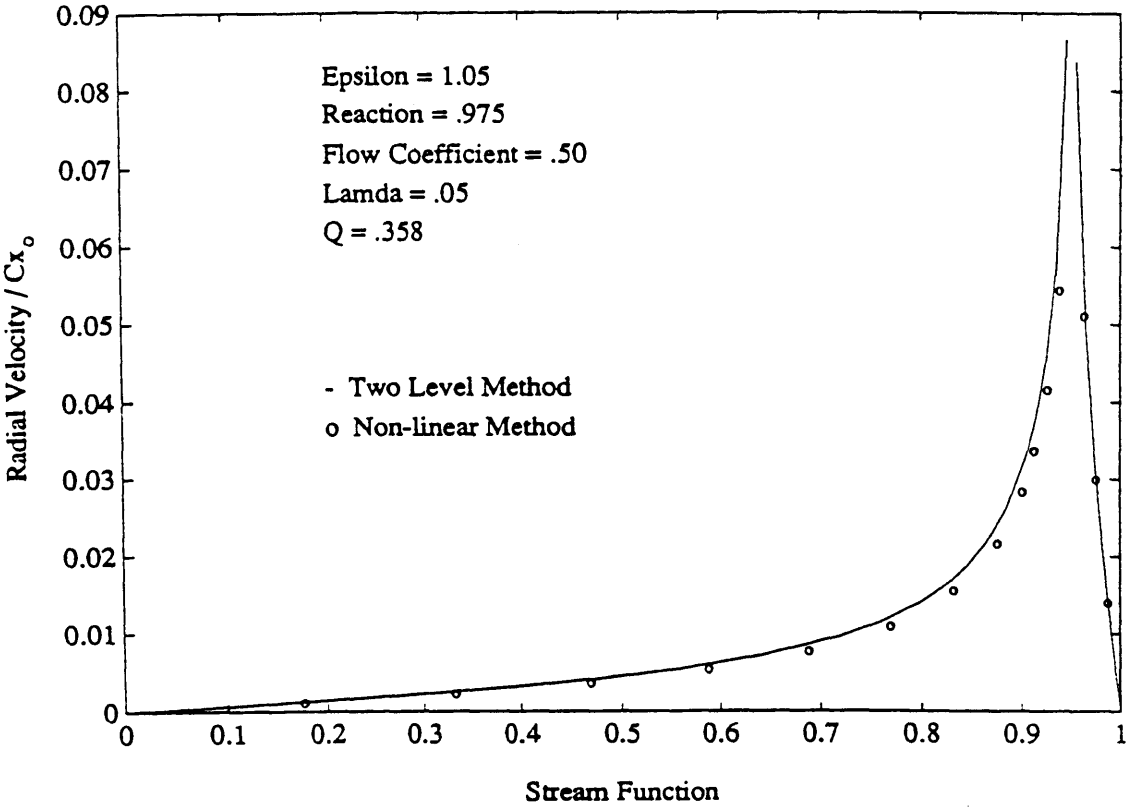

Fig. 26: Numerical vs. analytical spanwise velocity profiles at disk

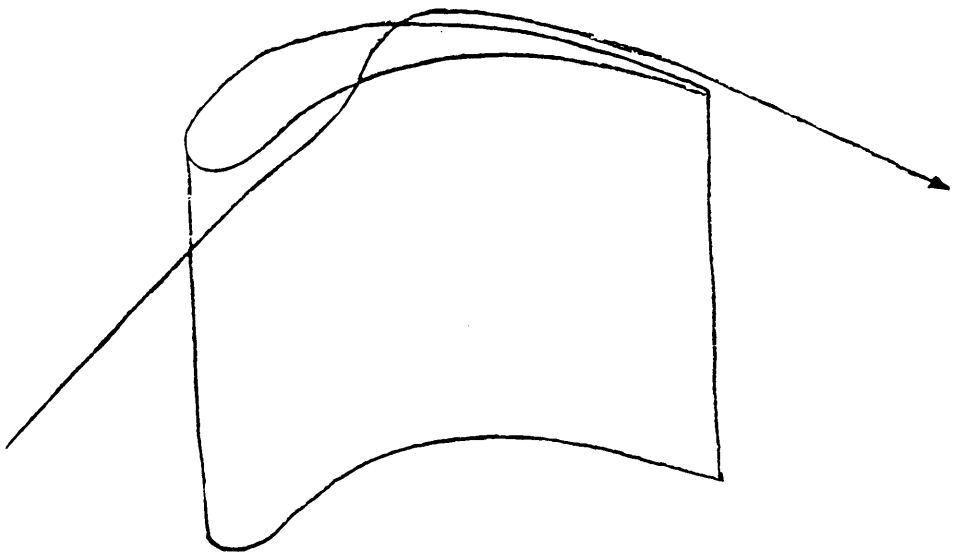

Fig. 27: Gap fluid does some work on the rotor

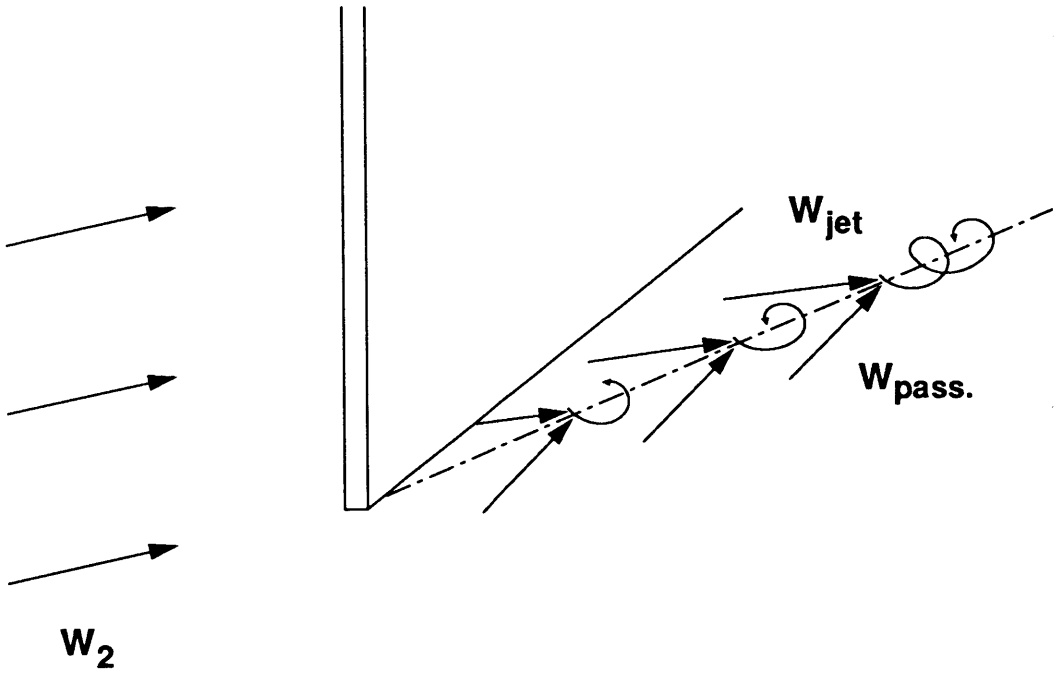

Fig. 28: Schematic of the colliding leakage jet and passage flows

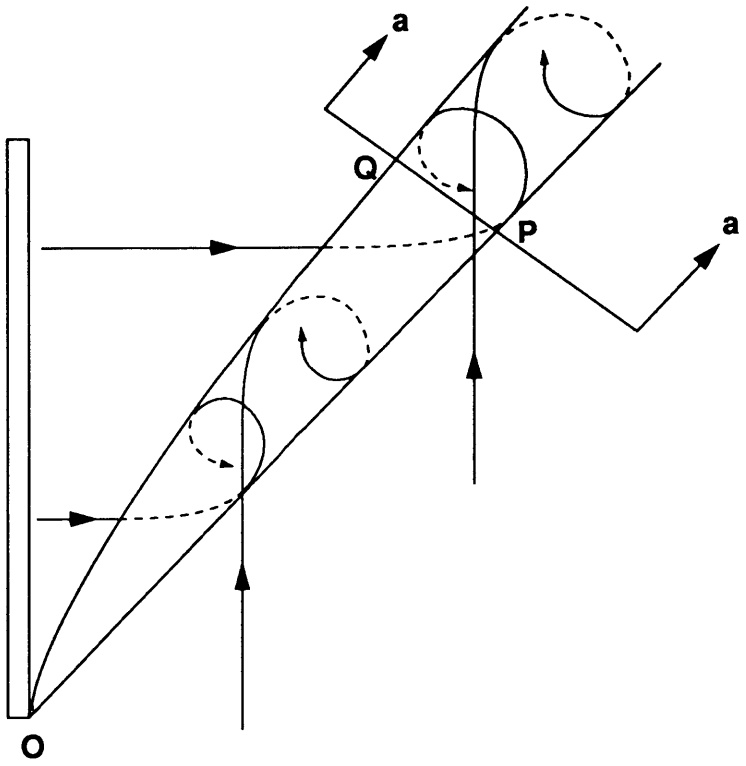

Fig. 29: Planform view of Fig. 28

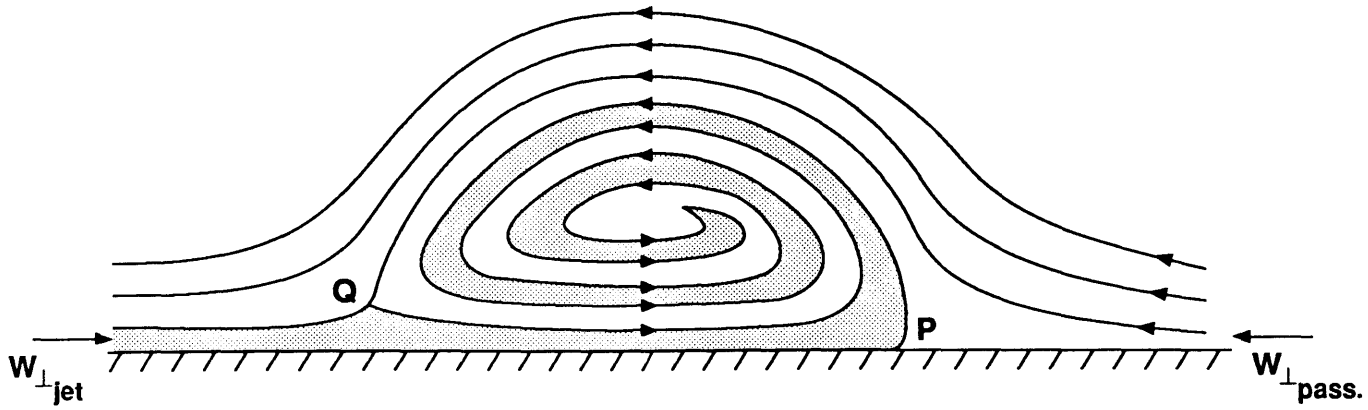

a-a View (Perpendicular to OP)

Fig. 30: Flow pattern in line a-a of Fig. 29

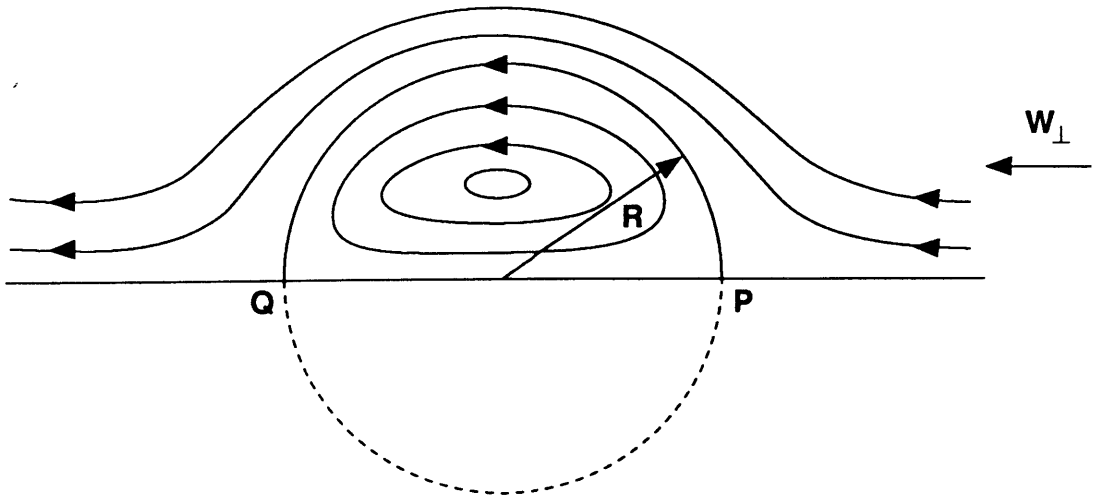

Fig. 31: Coordinates for model vortex

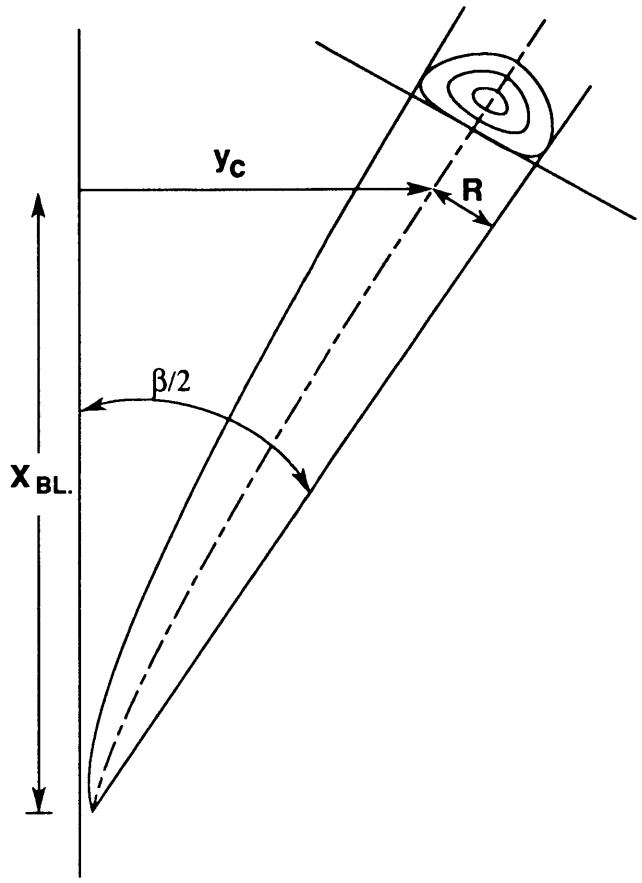

Fig. 32: Position and width of rolled-up leakage vortex

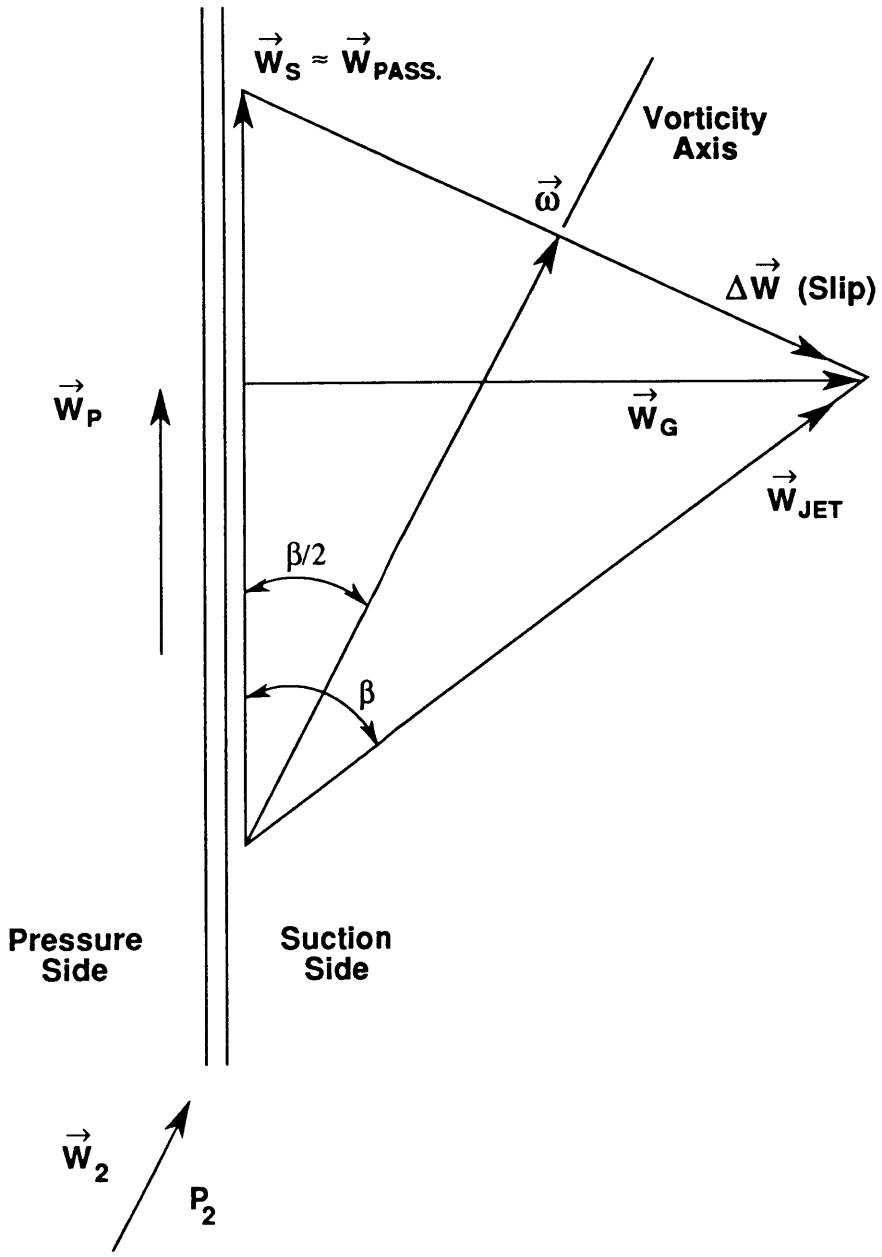

Fig. 33: Velocities and angles associated with roll-up

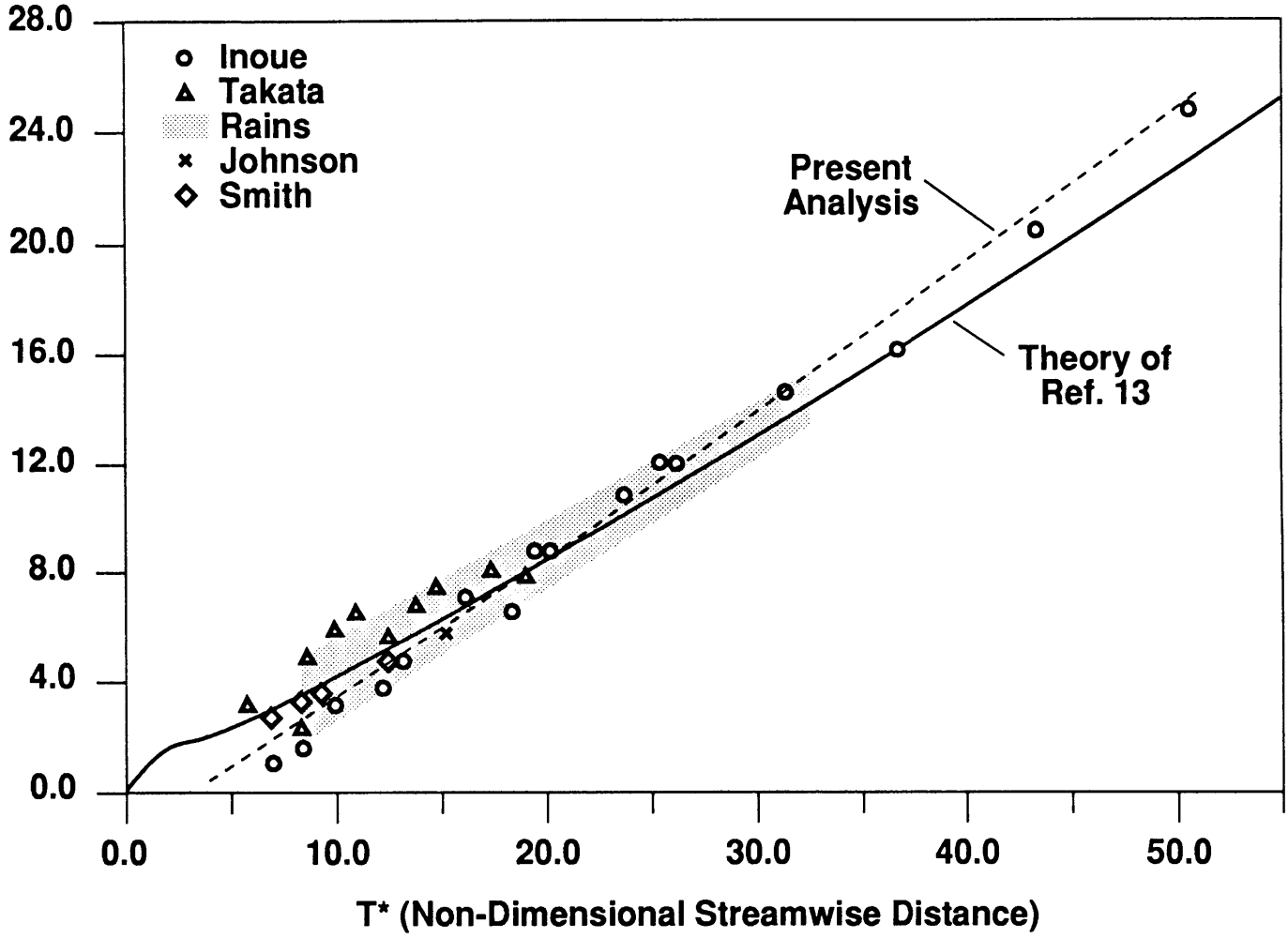

Fig. 34: Trajectory of vortex centroid compared to data and theory of Ref. 13

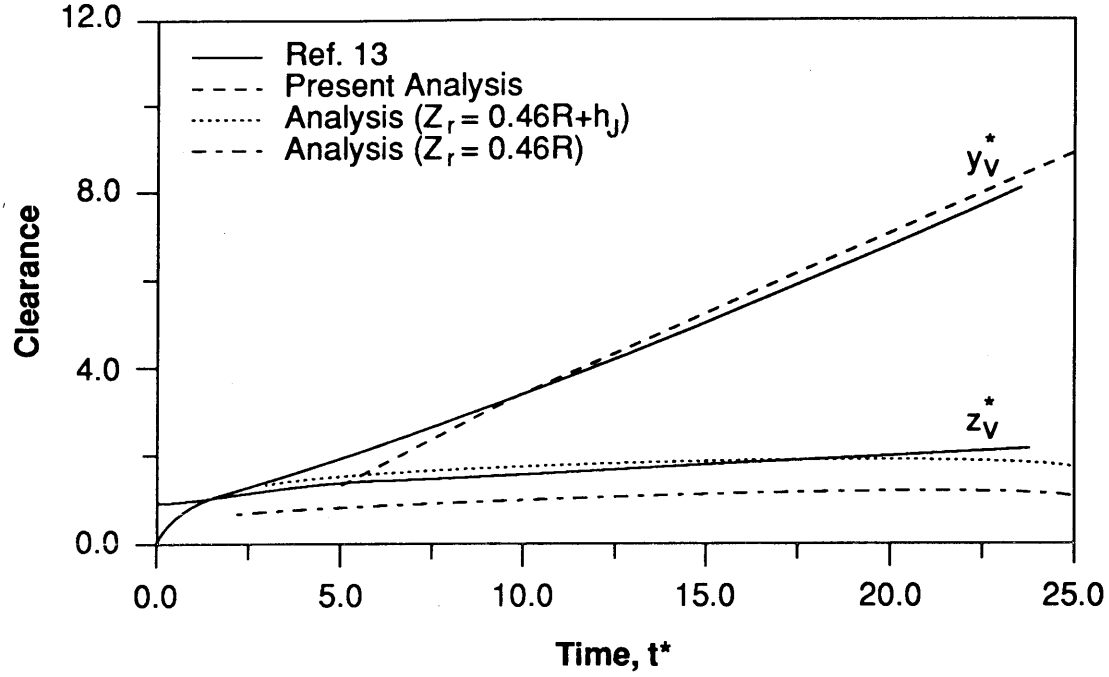

Fig. 35: Coordinates of vorticity centroid for tip clearance vortex